Relativistic calculations of the charge-transfer probabilities and cross sections for low-energy collisions of H-like ions with bare nuclei

I. I. Tupitsyn,[1] Y. S. Kozhedub,[1] V. M. Shabaev,[1] G. B. Deyneka,[2] S. Hagmann,[3] C. Kozhuharov,[3] G. Plunien,[4] and Th. Stöhlker[3,5,6]

[1]*Department of Physics, St. Petersburg State University, Ulianovskaya 1, Petrodvorets, 198504 St. Petersburg, Russia*
[2]*St. Petersburg State University of Information Technologies, Mechanics and Optics, Kronverk av. 49, 197101 St. Petersburg, Russia*
[3]*GSI Helmholtzzentrum für Schwerionenforschung GmbH, Planckstrasse 1, D-64291 Darmstadt, Germany*
[4]*Institut für Theoretische Physik, Technische Universität Dresden, Mommsenstraße 13, D-01062 Dresden, Germany*
[5]*Physikalisches Institut, Universität Heidelberg, Philosophenweg 12, D-69120 Heidelberg, Germany*
[6]*Helmholtz-Institut Jena, D-07743 Jena, Germany*

(Received 24 May 2010; published 7 October 2010)

A method for solving the time-dependent two-center Dirac equation is developed. The time-dependent Dirac wave function is represented as a sum of atomiclike Dirac-Sturm orbitals, localized at the ions. The atomic orbitals are generated by solving numerically the one-center Dirac and Dirac-Sturm equations by means of a finite-difference approach with the Coulomb potential taken as the sum of the exact reference-nucleus potential and of the other nucleus within the monopole approximation. An original procedure for calculating the two-center integrals with these orbitals is proposed. As a first test of the approach developed here, calculations of the charge-transfer and ionization cross sections for the H($1s$)-proton collisions at proton energies from 1 to 100 keV are performed. The obtained results are compared with related experimental and other theoretical data. To investigate the role of the relativistic effects, the charge-transfer cross sections in collisions of $Ne^{9+}(1s)$-Ne^{10+} (at energies from 0.1 to 10 MeV/u) and $U^{91+}(1s)$-U^{92+} (at energies from 6 to 10 MeV/u) are calculated for both relativistic and nonrelativistic cases.

DOI: 10.1103/PhysRevA.82.042701 PACS number(s): 34.10.+x, 34.50.−s, 34.70.+e

I. INTRODUCTION

Since the pioneering works [1–3], where the oscillatory behavior of the resonance charge-transfer probability for low-energy collisions was predicted, numerous publications have been devoted to the theoretical investigations of the charge transfer, excitations, and ionization in the H($1s$)-H^+ collisions (see, e.g., reviews [4–6]). Nonrelativistic two-center finite basis set calculations have been carried out in Refs. [7–13]. Nonrelativistic three-dimensional lattice methods in position as well as in momentum space have been applied for solving the time-dependent Schrödinger equation in Refs. [14–18]. Within the nonrelativistic approach, the probabilities and cross-sections for a homonuclear collision $A^{(Z-1)+}(1s)$-A^{Z+} for the nuclear charge $Z > 1$ can be easily obtained by scaling to the H($1s$)-H^+ collision. In the straight-line trajectory approximation, the cross section $\sigma(Z,v)$ scales exactly as $\sigma(Z,v) = \sigma(1,v/Z)/Z^2$ [4,19], where v is the projectile velocity. This scaling law, however, is not valid within the relativistic theory.

Collisions involving highly charged ions allow for sensitive tests of relativistic and quantum electrodynamics effects in scattering processes [20–22]. The study of such scenarios could provide also a unique tool to probe quantum electrodynamics (QED) in supercritical external Coulomb fields, if the total charge of the colliding ions $Z = Z_A + Z_B$ is larger than the critical value $Z_c \simeq 173$ (see, e.g., Refs. [23–26] and references therein). In the presence of such strong fields the energy of the one-electron $1\sigma_+$ state of the quasimolecule can reach the negative-energy Dirac continuum, when the internuclear distance R between target ion A and projectile ion B approaches the critical value R_c. For distances R less than R_c the ground-state level dives into the negative-continuum spectrum. In the $U^{91+}(1s)$-U^{92+} collision the critical radius for the point nucleus case was found to be $R_c = 36.8$ fm [27].

To date, various approaches were developed to treat the problem of heavy-ion collisions [28]. In Refs. [29–36], the two- and three-dimensional numerical lattice methods were employed to solve the time-dependent Dirac equation at high energies. In Refs. [37–40], high-energy relativistic collisions of heavy ions were considered using the basis set approach, in which the time-dependent wave function was expanded in terms of the atomic eigenstates of the projectile and the target. For internuclear distances smaller than about 1000 fm, some effects can also be evaluated within the so-called monopole approximation, which accounts only for the spherically symmetric part of the two-center potential (see, e.g., Refs. [41–43]). The atomic processes such as excitation, ionization, and charge transfer in relativistic atomic collisions involving heavy and highly charged projectile ions with energies ranging from 100 MeV/u upward were studied in Refs. [20,34,36,44–46] and references therein.

In the present work, we develop a method for solving the stationary and time-dependent two-center Dirac equation. The wave functions are expanded in terms of Dirac and Dirac-Sturm basis functions, which are central-field four-component Dirac bispinors centered at the ions. The radial parts of these orbitals are obtained by solving numerically the finite-difference radial one-center Dirac and Dirac-Sturm equations. In nonrelativistic calculations for atoms and molecules, the so-called Coulomb-Sturmian basis set was introduced in Ref. [47]. The Hartree-Fock calculations of atoms with this basis were considered by many authors (see, e.g., Ref. [48]). The relativistic Coulomb-Sturmian basis was employed in Refs. [49–52]. In the present article we use a non-Coulomb relativistic Sturm basis set, which is obtained by solving

 ©2010 The American Physical Society

numerically the Dirac-Sturm equations with a special choice of the weight function, as was proposed in Refs. [53,54]. This allows us to include any central-field potential in the radial equations for the large and small components of the basis functions. In particular, the Coulomb potential of the other ion can be included in the radial equations within the monopole approximation. The basis set constructed in this way is described in detail in Sec. II B.

Efficient evaluations of two-center integrals with the basis functions employed will require special tools. In the nonrelativistic case, a special symmetrical procedure for such calculations, based on the Löwdin reexpansion [55], was developed in Refs. [56,57]. In Sec. II C, we generalize this procedure to the relativistic case.

Within our approach, we use two basis sets of different size, in the following referred to as Basis 1 (medium) and Basis 2 (extended), respectively. The medium size Basis 1 is used for solving both the stationary and time-dependent Dirac equation. The extended Basis 2, due to high requirements to computer resources, is employed only in calculations of the stationary states of quasimolecules. The specific choice of these basis sets will be described in Sec. III A.

To test the quality of the two-center expansion described previously, we perform relativistic calculations for the ground-state energy of the molecular ion $H_2{}^+$ and the one-electron quasimolecule $Th_2{}^{179+}$ at the "chemical" distance $R = 2/Z$ (in a.u.) and compare the results with high-precision calculations presented in Refs. [58,59]. Treating the ground-state energy as a function of the internuclear distance R, we determine the critical radii R_c for a number of one-electron quasimolecules, including the system $U_2{}^{183+}$. Most calculations of the critical distances R_c presented in the literature were performed either for the pointlike nuclei [27,60,61] or with rather crude estimates of the nuclear-size effects [62–64]. We calculate the critical distances for both pointlike and extended nuclear charge density distributions using the same basis-set expansion. The results obtained here, as well as a comparison with calculations performed by other authors, are presented in Sec. III B.

For the collision energies under consideration, the electron dynamics has to be described quantum mechanically while the ion motion can be treated classically as the motion of point charges. Solving Newton's equations yields the classical Rutherford trajectories [25] of the projectile and target ions. In this article, in the collision of a neutral hydrogen atom with the proton, we used the straight-line trajectory with constant velocity for the projectile, while the target is at rest. The collision of highly charged ions with a bare nucleus was considered as a motion of the projectile and target along nonlinear Rutherford trajectories. The straight-line trajectory was also used in the nonrelativistic limit for comparison with scaling law data. In our calculations we used the rest coordinate system with respect to the initial position of the target.

The Born-Oppenheimer approximation is used to separate the motion of the electron and the nuclei. The magnetic interaction between the electron and the moving ions is neglected, because of low velocity of the projectile with respect to the target. The time-dependent Dirac equation for the electron is solved using the two-center basis-set expansion. The expansion coefficients can be defined employing, for example, the Crank-Nicholson propagation scheme [65] or the split-operator method [66]. These methods preserve the norm of the time-dependent wave function at each time step, since the Crank-Nicholson operator and the split-operator are unitary. However, in this work we use the direct evolution (exponential) operator method, which is more stable compared to the others. To obtain the matrix representation of the exponential operator in the finite basis set, one has to diagonalize the generalized Hamiltonian matrix at each time step. Since our basis set is not too large, the diagonalization procedure is not too time consuming. The amplitudes of the charge transfer to different bound states of the projectile ion are calculated nonperturbatively by projecting the time-dependent wave function onto the moving ("traveling") Dirac orbitals of the projectile.

In Sec. III C we present the results of the relativistic calculations of the charge-transfer probabilities and cross sections for the $H(1s)$-H^+, $Ne^{9+}(1s)$-Ne^{10+}, $Xe^{53+}(1s)$-Xe^{54+}, and $U^{91+}(1s)$-U^{92+} low-energy collisions. All the calculations are performed in the laboratory frame S, that is defined to be at rest with respect to the initial target position. The $H(1s)$-H^+ collision is considered in Sec. III C 1. Since the relativistic effects in this collision are negligible, the results of our calculations can be compared with nonrelativistic data obtained by other authors (Sec. III C 1). The role of the relativistic effects is investigated in Secs. III C 2, III C 3, and III C 4, where the relativistic and nonrelativistic calculations of the charge-transfer probabilities and cross sections are performed for higher-Z ions.

II. THEORY

A. Two-center Dirac equation in the finite basis set

1. Two-center expansion

Within the Born-Oppenheimer approximation, the motion of the electron is considered as a motion in the field of the two nuclei being at given positions (the stationary case) or moving along the classical trajectories (the nonstationary case). Let $\boldsymbol{R}_A$ and $\boldsymbol{R}_B$ denote the positions of the target (A) and projectile (B) nuclei, respectively. The time-dependent $\Psi(\boldsymbol{r},t)$ and stationary $\psi(\boldsymbol{r})$ wave functions are the solutions of the time-dependent and stationary Dirac equations, respectively. In atomic units ($\hbar = m = e = 1$), these equations are given by

$$i\frac{\partial\Psi(\boldsymbol{r},t)}{\partial t} = \hat{h}_{\rm D}\Psi(\boldsymbol{r},t), \quad \hat{h}_{\rm D}\psi_n(\boldsymbol{r}) = \varepsilon_n\psi_n(\boldsymbol{r}). \tag{1}$$

Here ε_n is the energy of the stationary state and the $\hat{h}_{\rm D}$ is the two-center Dirac Hamiltonian defined by

$$\hat{h}_{\rm D} = c(\boldsymbol{\alpha}\cdot\boldsymbol{p}) + \beta c^2 + V_{AB}(\boldsymbol{r}), \tag{2}$$

where c is the speed of light, $\boldsymbol{\alpha}$ and β are the Dirac matrices, and

$$\begin{aligned} V_{AB}(\boldsymbol{r}) &= V^A_{\rm nucl}(\boldsymbol{r}_A) + V^B_{\rm nucl}(\boldsymbol{r}_B),\\ \boldsymbol{r}_A &= \boldsymbol{r} - \boldsymbol{R}_A,\\ \boldsymbol{r}_B &= \boldsymbol{r} - \boldsymbol{R}_B, \end{aligned} \tag{3}$$

$$V_{\rm nucl}(\boldsymbol{r}) = \begin{cases} -Z/r & \text{for the point nucleus,}\\ \int d^3\boldsymbol{r}'\frac{\rho_{\rm nucl}(\boldsymbol{r}')}{|\boldsymbol{r}-\boldsymbol{r}'|} & \text{for the extended nucleus.}\end{cases} \tag{4}$$

The nuclear charge density $\rho_{\rm nucl}(\boldsymbol{r})$ is defined by the nuclear model. In this article, we use the Fermi model for the nuclear charge-density distribution.

Here and in what follows we consider only the electric part of the classical electromagnetic interaction between the electron and the moving nuclei, neglecting the magnetic interaction $[e/c\boldsymbol{A}(\boldsymbol{r})]$, which is small for low-energy collisions.

The two-center expansion of the stationary wave function $\psi_n(\boldsymbol{r})$ and the time-dependent wave function $\Psi(\boldsymbol{r},t)$ can be written in the form

$$\begin{aligned}\psi_n(\boldsymbol{r}) &= \sum_{\alpha=A,B}\sum_a c^n_{\alpha a}\varphi_{\alpha,a}(\boldsymbol{r}-\boldsymbol{R}_\alpha),\\ \Psi(\boldsymbol{r},t) &= \sum_{\alpha=A,B}\sum_a C_{\alpha a}(t)\varphi_{\alpha,a}\boldsymbol{(r}-\boldsymbol{R}_\alpha(t)\boldsymbol{)},\end{aligned} \tag{5}$$

where index $\alpha = A,B$ labels the centers, index a enumerates basis functions at the given center, and $\varphi_{\alpha,a}(\boldsymbol{r}-\boldsymbol{R}_\alpha)$ is the central-field bispinor, centered at point α. (In what follows, the shorthand notation $|i\rangle = |\varphi_i\rangle \equiv |\varphi_{\alpha,a}\rangle$ for state vectors, respectively, $i \equiv \alpha, a$ is also used.) The coefficients $c^n_{a\alpha}$ of the expansion (5) for the stationary wave function $\psi_n(\boldsymbol{r})$ can be obtained from the generalized eigenvalue equation,

$$\sum_k H_{jk}c^n_k = \varepsilon_n \sum_k S_{jk}c^n_k, \tag{6}$$

where indices j and k enumerate the basis functions of both centers, and the matrix elements of H and S are given by

$$H_{jk} = \langle j|\hat{h}_{\rm D}|k\rangle, \quad S_{jk} = \langle j|k\rangle. \tag{7}$$

The expansion coefficients $C_{a\alpha}(t)$ of the time-dependent wave function $\Psi(\boldsymbol{r},t)$ can be obtained by solving the linear system of first-order differential equations,

$$i\sum_k S_{jk}\frac{dC_k(t)}{dt} = \sum_k (H_{jk}-T_{jk})C_k(t). \tag{8}$$

The matrix elements of T are given by

$$T_{jk} = i\langle j|\frac{\partial}{\partial t}|k\rangle = T^*_{kj} + i\frac{\partial}{\partial t}S_{jk}. \tag{9}$$

Obviously, the matrix T is non-Hermitian if the overlapping matrix S depends on time.

The functions $\varphi_{\alpha,a}$ depend on time due to two reasons. First, the basis functions centered at the target and projectile nuclei move together with the nuclei. Second, the basis functions depend parametrically on the distance between the nuclei, since their radial parts are obtained from the radial equations, where for each center the potential of the other nucleus is included in the so-called monopole approximation (see Sec. II B). Therefore, the time derivative of the basis function

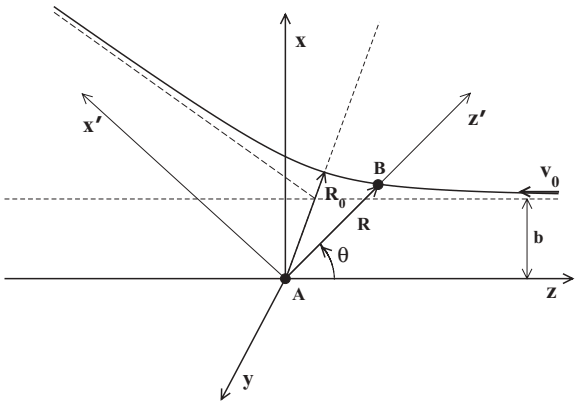

FIG. 1. The hyperbolic Rutherford trajectory (b is the impact parameter, R_0 is the minimal distance between target A and projectile B, $\boldsymbol{v}_0$ is the initial projectile velocity). The coordinate system $S_{\rm t} = (x,y,z)$ is defined with respect to the moving target ion.

can be divided into two parts:

$$\langle j|\frac{\partial}{\partial t}|k\rangle = \frac{dR}{dt}\left\langle\varphi_j\left|\frac{\partial\varphi_k}{\partial R}\right.\right\rangle - \boldsymbol{v}_{\alpha_k}\cdot\langle\varphi_j|\nabla|\varphi_k\rangle, \tag{10}$$

where $\boldsymbol{v}_\alpha = d\boldsymbol{R}_\alpha/dt$ is the velocity of the ion α.

2. *Trajectories of nuclear motion*

For simplicity let us consider here (only in this subsection) the coordinate system defined with respect to the moving target ion. In the ion-ion collisions the internuclear distance vector $\boldsymbol{R} = \boldsymbol{R}_B - \boldsymbol{R}_A$, respectively its length $R = |\boldsymbol{R}|$, the target velocity ($\boldsymbol{v}_A$), and the projectile velocity ($\boldsymbol{v}_B$) are dependent on time. This dependence is defined by the trajectories of the nuclear motion. In low-energy collisions the nuclear trajectories can be obtained by solving classical nonrelativistic Newton's equations of motion. In the case of point charges, this solution is a well-known Rutherford hyperbola (see Fig. 1), which can be given in the parametric representation by the equations [25]

$$\begin{aligned}R &= a(\varepsilon\cosh\xi + 1),\\ t &= \frac{a}{v_0}(\varepsilon\sinh\xi + \xi),\end{aligned} \tag{11}$$

where $\xi \in (-\infty,\infty)$,

$$a = \frac{Z_A Z_B e^2}{M_{\rm r}v_0^2}, \quad \varepsilon = \left(1+\frac{b^2}{a^2}\right)^{1/2}, \tag{12}$$

v_0 is the initial velocity of the projectile, b is the impact parameter, and $M_{\rm r}$ is the reduced ion mass. In the coordinate system $S_{\rm t} = (x,y,z)$, which is shown in Fig. 1, the X and Z components of the internuclear distance vector $\boldsymbol{R}$ are given by

$$\begin{aligned}Z &= R\cos\theta,\\ X &= R\sin\theta,\end{aligned} \quad \text{where} \quad \theta = 2\arctan\left[\frac{\sqrt{\varepsilon^2-1}[\tanh(\xi/2)+1]}{(\varepsilon+1)-(\varepsilon-1)\tanh(\xi/2)}\right]. \tag{13}$$

The angle θ is related to the scattering angle Θ_∞ by $\Theta_\infty = \pi - \theta(t=\infty)$.

It should be noted that, in fact, in our calculations we used a fixed coordinate system with respect to the initial position of the target. In contrast to the moving target frame, this system is an inertial one.

3. *Matrix form of the time-dependent Dirac equation*

In this work the two-center basis set φ_j is not orthonormal. Let us consider the transformation of the basis set φ_j to the orthonormal basis φ_j^L by a matrix L^{-1}:

$$\varphi_j^L = \sum_k L_{kj}^{-1}\varphi_k, \quad \varphi_j = \sum_k L_{kj}\varphi_k^L. \tag{14}$$

Then the positive-definite matrix S can be represented as the product of L^+ and L:

$$S = L^+L,$$
$$S_{jk}^L = \langle\varphi_j^L|\varphi_k^L\rangle = \langle\varphi_j|L^{-1^+}SL^{-1}|\varphi_j\rangle = (L^{-1^+}SL^{-1})_{jk} = \delta_{j,k}. \tag{15}$$

If the matrix L is an upper-triangle matrix, then the decomposition (15) is so-called Cholesky factorization [67]. The expansion of the time-dependent wave function over the orthonormal basis φ_j^L is given by

$$\Psi(\boldsymbol{r},t) = \sum_{\alpha=A,B}\sum_a C_{\alpha,a}^L(t)\varphi_{\alpha,a}^L(\boldsymbol{r}-\boldsymbol{R}_\alpha(t),t), \tag{16}$$

where $\boldsymbol{C}^L = L\boldsymbol{C}$.

With respect to the basis φ_j^L, the time-dependent Dirac equation can be equivalently expressed in the matrix (differential) equation

$$i\frac{d\boldsymbol{C}^L(t)}{dt} = M\boldsymbol{C}^L(t), \tag{17}$$

where $M = H^L - T^L$, the Hermitian Hamiltonian matrix H^L is

$$H_{ij}^L = \langle\varphi_i|\hat{H}|\varphi_j\rangle = (L^{-1^+}HL^{-1})_{ij}, \tag{18}$$

and the matrix T^L is defined by

$$T_{ij}^L = \langle\varphi_i^L|\hat{T}|\varphi_j^L\rangle = (L^{-1^+}TL^{-1})_{ij} + i\left(L\frac{dL^{-1}}{dt}\right)_{ij}$$
$$= \left[L^{-1^+}\left(T - iL^+\frac{dL}{dt}\right)L^{-1}\right]_{ij}. \tag{19}$$

It should be noted that the matrix T^L is Hermitian, in contrast to the matrix T defined by Eq. (9). Therefore, the matrix M is also Hermitian.

The time-dependent matrix equation (17) can be considered as a linear system of coupled first-order differential equations for the expansion coefficients $\boldsymbol{C}^L$ over the entire range of time $t \in (-\infty,\infty)$. We assume that at the initial moment of time ($t \to -\infty$) the electron is bound in the $1s$ state of the target, while the projectile is a bare nucleus. Then the wave function $\Psi(\boldsymbol{r},t)$ at $t \to -\infty$ is given by

$$\Psi(\boldsymbol{r},t)|_{t\to-\infty} = \psi_{1s}(\boldsymbol{r}). \tag{20}$$

If the Dirac $1s$ target wave function $\psi_{1s}(\boldsymbol{r})$ is included in the basis set, the initial conditions for the expansion coefficients can be written as

$$C_j^L(t)|_{t\to-\infty} = C_j(t)|_{t\to-\infty} = \delta_{j,1s}. \tag{21}$$

Equation (17) is solved numerically, using the approximate evolution operator

$$\boldsymbol{C}^L(t+\Delta t) = e^{-i\overline{M}t}\boldsymbol{C}^L(t) + O(\Delta^3 t), \tag{22}$$

where Hermitian matrix $\overline{M}$ is chosen as

$$\overline{M} = M(t+\Delta t/2). \tag{23}$$

Since the approximate evolution operator $U(t) = \exp(-i\overline{M}t)$ is unitary, the time-dependent wave function preserves the norm at each time step:

$$\langle\Psi(\boldsymbol{r},t)|\Psi(\boldsymbol{r},t)\rangle = \sum_j \left|C_j^L(t)\right|^2 = 1. \tag{24}$$

The matrix $e^{-i\overline{M}t}$ is calculated at each time step using the eigendecomposition of matrix $\overline{M}$,

$$\overline{M} = V\Lambda V^+, \quad \Lambda = V^+\overline{M}V, \tag{25}$$

where Λ is a diagonal matrix and columns of matrix V are the eigenvectors of $\overline{M}$. Then one obtains

$$e^{-i\overline{M}t} = Ve^{-i\Lambda t}V^+. \tag{26}$$

The time grid points t_i are chosen as $t_i = a/v_0(\varepsilon\sinh\xi_i + \xi_i)$, where the parameter ξ is discretized over a uniform grid. The corresponding grid points R_i can be obtained using Eq. (11).

B. Basis functions

In our approach the basis set contains Dirac and Dirac-Sturm orbitals. The Dirac-Sturm orbitals can be considered as pseudostates, which should be included in the basis to take into account the contribution of the positive- and negative-energy Dirac continuum. Both types of basis functions $\varphi_{\alpha a}$ are central field Dirac bispinors centered at the position of either ion $\boldsymbol{R}_\alpha$ ($\alpha = A,B$),

$$\varphi_{n\kappa m}(\boldsymbol{r}) = \begin{pmatrix} \dfrac{P_{n\kappa}(r)}{r}\chi_{\kappa m}(\Omega,\sigma) \\ i\dfrac{Q_{n\kappa}(r)}{r}\chi_{-\kappa m}(\Omega,\sigma) \end{pmatrix}, \tag{27}$$

where $P_{n\kappa}(r)$ and $Q_{n\kappa}(r)$ are large and small radial components, respectively, and $\kappa = (-1)^{l+j+1/2}(j+1/2)$ is the relativistic angular quantum number. The large and small radial orbital components are obtained by solving numerically the Dirac or Dirac-Sturm equations in the central field potential $V(r)$. The radial Dirac equation for the radial components of the Dirac orbitals $\varphi_{n\kappa m}$ is given by

$$c\left(-\frac{d}{dr} + \frac{\kappa}{r}\right)Q_{n\kappa}(r) + (V(r)+c^2)P_{n\kappa}(r) = \varepsilon_{n\kappa}P_{n\kappa}(r),$$
$$c\left(\frac{d}{dr} + \frac{\kappa}{r}\right)P_{n\kappa}(r) + (V(r)-c^2)Q_{n\kappa}(r) = \varepsilon_{n\kappa}Q_{n\kappa}(r). \tag{28}$$

The radial components of the Dirac-Sturm orbitals $\overline{\varphi}_{n\kappa m}$ which we denote by $\overline{P}_{n\kappa}(r)$ and $\overline{Q}_{n\kappa}(r)$, are the solutions of the

generalized Dirac-Sturm eigenvalue equation:

$$\begin{aligned} c\left(-\frac{d}{dr}+\frac{\kappa}{r}\right)\overline{Q}_{n\kappa}(r)+\left(V(r)+c^2-\varepsilon_{n_0\kappa}\right)\overline{P}_{n\kappa}(r)&=\lambda_{n\kappa}W_\kappa(r)\overline{P}_{n\kappa}(r),\\ c\left(\frac{d}{dr}+\frac{\kappa}{r}\right)\overline{P}_{n\kappa}(r)+\left(V(r)-c^2-\varepsilon_{n_0\kappa}\right)\overline{Q}_{n\kappa}(r)&=\lambda_{n\kappa}W_\kappa(r)\overline{Q}_{n\kappa}(r). \end{aligned} \tag{29}$$

Here $\lambda_{n\kappa}$ can be considered as the eigenvalue of the Dirac-Sturm operator and $W_\kappa(r)$ is a constant-sign weight function. The energy $\varepsilon_{n_0\kappa}$ is fixed in the Dirac-Sturm equation. If $W(r)\to 0$ at $r\to\infty$, all Sturmian functions have the same asymptotic behavior at $r\to\infty$. It is clear that for $\lambda_{n\kappa}=0$ the Sturmian function $\overline{\varphi}_{n\kappa m}$ coincides with the reference Dirac orbital $\varphi_{n\kappa m}$ which has the radial parts $P_{n_0\kappa}(r)$ and $Q_{n_0\kappa}(r)$. The widely known choice of the weight function is $W(r)=1/r$, which leads to the well known "charge quantization" $Z^*_{n\kappa}=Z+\lambda_{n\kappa}$. For a Coulomb potential $V(r)=-Z/r$, the main advantage of this choice is that the Coulomb-Sturmian orbitals can be given in an analytical form. This is not the case, however, for a non-Coulomb potential $V(r)$. In the relativistic case the choice $W(r)=1/r$ is not very successful, because of the incorrect behavior of the Coulomb-Sturmian orbitals at $r\to 0$. For this reason the standard form of the equation has to be modified [50,68,69].

In our calculations we use the following weight function:

$$W_\kappa(r)=-\frac{1-\exp[-(\alpha_\kappa r)^2]}{(\alpha_\kappa r)^2}. \tag{30}$$

In contrast to $1/r$, this weight function is regular at the origin. It is well-known that the Sturmian operator is Hermitian and does not contain continuous spectra, in contrast to the Dirac operator. Therefore, the set of the Sturmian eigenfunctions forms a discrete and complete basis set of one-electron wave functions.

The central-field potential $V(r)$ in Eqs. (28) and (29) is arbitrary, and, therefore, it can be chosen to provide most appropriate Dirac and Dirac-Sturm basis orbitals. At small internuclear distances the wave function of the electron experiences the strong Coulomb field of both nuclei. To leading order this effect is taken into account by inclusion of the Coulomb potential of the second ion in the total one center potential $V(r)$ within the so-called monopole approximation. For instance, the total central-field potential $V^A(r)$ of the center A is given by

$$V^A(r)=V^A_{\rm nucl}(r)+V^B_{\rm mon}(r), \tag{31}$$

where $V^A_{\rm nucl}(r)$ is the Coulomb potential of the nucleus A and $V^B_{\rm mon}(r)$ is the spherically symmetric part of the reexpansion of the potential $V^B_{\rm nucl}(\boldsymbol{r}-\boldsymbol{R}_B)$ with respect to the center A

$$V^B_{\rm mon}(r)=\frac{1}{4\pi}\int d\Omega_A V^B_{\rm nucl}(\boldsymbol{r}-\boldsymbol{R}_B). \tag{32}$$

Note that $\boldsymbol{R}_B$ then is equal to the internuclear distance vector. For the point nucleus the potential $V^B_{\rm mon}(r)$ is given by

$$V^B_{\rm mon}(r)=\begin{cases}-\frac{Z_B}{r}, & r\geqslant R,\\ -\frac{Z_B}{R}, & r<R.\end{cases} \tag{33}$$

C. Two-center integrals

The one-center matrix elements of matrices H and S [Eq. (7)] are easily reduced to radial integrals [70], which are calculated by numerical integration over a semilogarithmic radial grid [71].

1. *Modified Löwdin reexpansion procedure*

The two-center matrix elements are evaluated using a symmetrical reexpansion procedure as proposed in Refs. [56, 57]. The reexpansion procedure is based on the technique developed by Löwdin [55]. We assume that in the local coordinate frame the z axis is directed along the internuclear axis A-B (see Fig. 2). The following geometrical relations take place:

$$\begin{aligned} &\boldsymbol{r}_A=\boldsymbol{r}-\boldsymbol{R}_A,\quad \boldsymbol{r}_B=\boldsymbol{r}-\boldsymbol{R}_B,\quad \boldsymbol{R}=\boldsymbol{R}_B-\boldsymbol{R}_A,\\ &\cos\theta_A=\frac{r_A^2+R^2-r_B^2}{2Rr_A},\quad \cos\theta_B=\frac{r_A^2-R^2-r_B^2}{2Rr_B}. \end{aligned} \tag{34}$$

Let the indices a and b enumerate basis functions centered at the points A and B, respectively. The standard Löwdin reexpansion of the nonrelativistic central-field function $F_b(\boldsymbol{r}_B)$ centered at the point B in terms of the spherical harmonics $Y_{lm}(\boldsymbol{r}_A)$ centered at the point A can be written in the form [55,72]

$$\begin{aligned} F_b(\boldsymbol{r}_B)&=\frac{f_b(r_B)}{r_B}Y_{l_bm_b}(\theta_B,\varphi)\\ &=\frac{1}{r_A}\sum_{l=0}^{\infty}\alpha_{lm_b}(f_b,l_b|r_A)Y_{lm_b}(\theta_A,\varphi), \end{aligned} \tag{35}$$

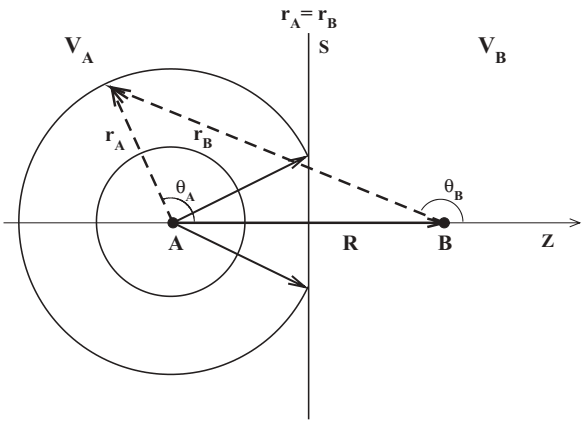

FIG. 2. Integration regions V_A and V_B.

where $\alpha_{lm_b}(f_b,l_b|r_A)$ is a so-called Löwdin α function defined by

$$\alpha_{lm_b}(f_b,l_b|r_A) = \frac{K_{l_b m_b} K_{l m_b}}{R} \int_{|r_A-R|}^{|r_A+R|} f_b(r) P_{l_b}^{|m_b|}\left(\frac{r_A^2-R^2-r^2}{2rR}\right) \times P_l^{|m_b|}\left(\frac{r_A^2+R^2-r^2}{2r_A R}\right) dr. \quad (36)$$

Here $P_l^{|m|}$ is the standard associated Legendre polynomial and K_{lm} is the normalization constant

$$K_{lm} = \sqrt{\frac{2l+1}{2}\frac{(l-|m|)!}{(l+|m|)!}}. \quad (37)$$

Similarly, the function $F_a(\boldsymbol{r}_A)$ centered at point A can be expanded in spherical harmonics $Y_{lm}(\theta_B,\varphi)$ centered at the point B.

When the logarithmic or semilogarithmic grid is used, the radial grid step increases with increasing radius r_A. Therefore, the Löwdin reexpansion procedure becomes unstable and poorly convergent for the values of radius r_A in the region near $r_A = R$, especially for the oscillating and strongly localized atomiclike wave functions. In addition, the Löwdin procedure is not symmetric with respect to the centers A and B.

To improve the convergence we modified the standard Löwdin reexpansion procedure by dividing the range of the integration into two regions V_A and V_B as shown in Fig. 2. The region V_A contains ion A and the region V_B contains ion B. The dividing of the integration area into two parts can be done, for example, by a plane passing through the center of the segment (AB). We apply the reexpansion procedure only to the "tails" of the wave functions occurring in a given region. To describe this procedure, we introduce the stepwise functions $\Theta_A(\boldsymbol{r})$ and $\Theta_B(\boldsymbol{r})$ by

$$\Theta_A(\boldsymbol{r}) = \begin{cases} 1, & \boldsymbol{r} \in V_A, \\ 0, & \boldsymbol{r} \in V_B, \end{cases} \qquad \Theta_B(\boldsymbol{r}) = \begin{cases} 0, & \boldsymbol{r} \in V_A, \\ 1, & \boldsymbol{r} \in V_B, \end{cases} \quad (38)$$

and rewrite the product of the functions centered at the different points in the following way:

$$F_a(\boldsymbol{r}_A)F_b(\boldsymbol{r}_B) = F_a(\boldsymbol{r}_A)[F_b(\boldsymbol{r}_B)\Theta_A(\boldsymbol{r})] + [F_a(\boldsymbol{r}_A)\Theta_B(\boldsymbol{r})]F_b(\boldsymbol{r}_B). \quad (39)$$

The reexpansion of the function tail $F_b(\boldsymbol{r}_B)\Theta_A(\boldsymbol{r})$ centered at B onto center A has the form

$$F_b(\boldsymbol{r}_B)\Theta_A(\boldsymbol{r}) = \frac{f_b(r_B)}{r_B} Y_{l_b m_b}(\theta_B,\varphi)\Theta_A(\boldsymbol{r}) = \frac{1}{r_A}\sum_l \overline{\alpha}_{lm_b}(f_b,l_b|r_A) Y_{lm_b}(\theta_A,\varphi), \quad (40)$$

where

$$\overline{\alpha}_{lm_b}(f_b,l_b|r_A) = \frac{K_{l_b m_b} K_{l m_b}}{R} \int_{r_>^A}^{|r_A+R|} f_b(r) P_{l_b}^{|m_b|}\left(\frac{r_A^2-R^2-r^2}{2rR}\right) \times P_l^{|m_b|}\left(\frac{r_A^2+R^2-r^2}{2r_A R}\right) dr \quad (41)$$

and $r_>^A = \max\{r_A,|r_A-R|\}$.

In the relativistic case the spin-angular part $\chi_{\kappa m}$ of the large and small components of the central-field wave function is the Pauli spinor [73]:

$$\chi_{\kappa\mu}(\boldsymbol{r},\sigma) = \chi_{ljm}(\boldsymbol{r},\sigma) = \sum_{m,m_s} C^{jm}_{lm,\frac{1}{2},m_s} Y_{lm}(\boldsymbol{r})\Phi_{m_s}(\sigma), \quad (42)$$

where $C^{jm}_{lm,\frac{1}{2},m_s}$ are the Clebsch-Gordan coefficients [74] and $\Phi_{m_s}(\sigma)$ is a spin function.

The symmetric reexpansion of the relativistic wave function tails onto centers A and B can be written in the form

$$\begin{pmatrix} \frac{P_b(r_B)}{r_B}\chi_{\kappa_b\mu_b}(\boldsymbol{r}_B) \\ i\frac{Q_b(r_B)}{r_B}\chi_{-\kappa_b\mu_b}(\boldsymbol{r}_B) \end{pmatrix} \Theta_A(\boldsymbol{r}) = \sum_\kappa \begin{pmatrix} \frac{\overline{p}_{\kappa\mu_b}(b|r_A)}{r_A}\chi_{\kappa\mu_b}(\boldsymbol{r}_A) \\ i\frac{\overline{q}_{-\kappa\mu_b}(b|r_A)}{r_A}\chi_{-\kappa\mu_b}(\boldsymbol{r}_A) \end{pmatrix} \quad (43)$$

and

$$\begin{pmatrix} \frac{P_a(r_A)}{r_A}\chi_{\kappa_a\mu_a}(\boldsymbol{r}_A) \\ i\frac{Q_a(r_A)}{r_A}\chi_{-\kappa_a\mu_a}(\boldsymbol{r}_A) \end{pmatrix} \Theta_B(\boldsymbol{r}) = \sum_\kappa (-1)^{l_a-l} \begin{pmatrix} \frac{\overline{p}_{\kappa\mu_a}(a|r_B)}{r_B}\chi_{\kappa\mu_a}(\boldsymbol{r}_B) \\ i\frac{\overline{q}_{-\kappa\mu_a}(a|r_B)}{r_B}\chi_{-\kappa\mu_a}(\boldsymbol{r}_B) \end{pmatrix}. \quad (44)$$

The $\overline{p}$ and $\overline{q}$ functions, which are the relativistic analogs of the modified Löwdin $\overline{\alpha}$ functions, are defined by

$$\overline{p}_{\kappa\mu_b}(b|r_A) = \sum_{m_b,m_s} C^{j_b\mu_b}_{l_b m_b,\frac{1}{2}m_s} C^{j\mu_b}_{lm_b,\frac{1}{2}m_s} \overline{\alpha}_{lm_b}(P_b,l_b|r_A),$$
$$\overline{q}_{\kappa\mu_b}(b|r_A) = \sum_{m_b,m_s} C^{j_b\mu_b}_{\bar{l}_b m_b,\frac{1}{2}m_s} C^{j\mu_b}_{\bar{l}m_b,\frac{1}{2}m_s} \overline{\alpha}_{\bar{l}m_b}(Q_b\bar{l}_b|r_A), \quad (45)$$

where $\bar{l} = l - \mathrm{sgn}(\kappa)$. The functions $\overline{\alpha}_{lm_b}(P_b,l_b|r_A)$ and $\overline{\alpha}_{\bar{l}m_b}(Q_b,\bar{l}_b|r_A)$ are defined by Eq. (41), where the function $f_b(r)$ has to be replaced by the functions $P_b(r)$ and $Q_b(r)$, respectively. The functions $\overline{p}_{\kappa\mu_a}(a|r_B)$ and $\overline{q}_{\kappa\mu_a}(a|r_B)$ are defined similarly to Eq. (45), where indices A and b should be replaced by B and a, respectively. Then the product of the two central-field big components centered at the different points (A and B) can be represented as the sum of two one-center products:

$$\frac{P_a(r_A)}{r_A}\chi_{\kappa_a\mu_a}(\boldsymbol{r}_A)\frac{P_b(r_B)}{r_B}\chi_{\kappa_b\mu_b}(\boldsymbol{r}_B) = \frac{P_a(r_A)}{r_A}\chi_{\kappa_a\mu_a}(\boldsymbol{r}_A)\left[\sum_\kappa \frac{\overline{p}_{\kappa\mu_b}(b|r_A)}{r_A}\chi_{\kappa\mu_b}(\boldsymbol{r}_A)\right] + \frac{P_b(r_B)}{r_B} \times \chi_{\kappa_b\mu_b}(\boldsymbol{r}_B)\left[\sum_\kappa (-1)^{l_a-l}\frac{\overline{p}_{\kappa\mu_a}(a|r_B)}{r_B}\chi_{\kappa\mu_a}(\boldsymbol{r}_B)\right]. \quad (46)$$

A similar expansion can be written for the product of the small components.

In this article the two-center overlap integrals $S^{(0)}_{ab}$ and matrix elements $H^{(0)}_{ab}$ and $G^{(0)}_{ab}$ of the Hamiltonian and gradient operators, respectively, are calculated using the symmetric reexpansion (46). Here and in what follows superscript (0) implies that the integral is considered in the local coordinate frame, where the z axis is directed along the internuclear axis A-B. The details of the calculation of the two-center integrals in the local coordinate system are presented in Appendix A.

2. Transformation of the two-center matrix elements to the laboratory frame

As indicated earlier, the laboratory frame S is defined to be at rest with respect to the initial target position. Then, the two-center matrix elements evaluated with respect to the local reference frame $S' = (x',y',z')$ (see Fig. 1) have to be transformed to the laboratory frame $S = (x,y,z)$. The corresponding two-center integrals can be obtained from $S^{(0)}_{ab}$, $H^{(0)}_{ab}$, and $G^{(0)}_{ab}$ by rotating the coordinate system around the y axis for angle $-\theta$ (Fig. 1). For the overlap integrals S_{ab} and the two-center Dirac-Hamiltonian matrix elements H_{ab} in the laboratory frame, S we obtain

$$S_{a,b} = S_{n_a\kappa_a\mu_a;n_b\kappa_b\mu_b} = \sum_{\mu} d^{j_a}_{\mu_a\mu}(\theta) d^{j_b}_{\mu_b\mu}{}^{*}(\theta) S^{(0)}_{n_a\kappa_a\mu;n_b\kappa_b\mu},$$
$$H_{a,b} = H_{n_a\kappa_a\mu_a;n_b\kappa_b\mu_b} = \sum_{\mu} d^{j_a}_{\mu_a\mu}(\theta) d^{j_b}_{\mu_b\mu}{}^{*}(\theta) H^{(0)}_{n_a\kappa_a\mu;n_b\kappa_b\mu}, \tag{47}$$

where $d^{j}_{\mu'\mu}(\theta)$ are real Wigner's D functions [74]. The transformation of the gradient matrix elements $G^{(0)}_{ab}(q)$ to the laboratory frame S is given by

$$G_{ab}(q) = G_{n_a\kappa_a\mu_a;n_b\kappa_b\mu_b}(q) = \sum_{\mu'_a,\mu'_b,q} d^{j_a}_{\mu_a\mu'_a}(\theta) d^{j_b}_{\mu_b\mu'_b}(\theta) d^{1}_{q'q}(\theta) G^{(0)}_{n_a\kappa_a\mu'_a;n_b\kappa_b\mu'_b}(q). \tag{48}$$

D. Charge-transfer probabilities and cross sections

1. Transition amplitudes

The transition amplitude for electron capture to an ion state αn is given by

$$T_{\alpha n}(t) = \langle \psi_{\alpha n}(\boldsymbol{r},t)|\Psi(\boldsymbol{r},t)\rangle, \quad t \to \infty. \tag{49}$$

As mentioned earlier, the index $\alpha = A,B$ labels different centers (target and projectile ions) and $\psi_{\alpha n}(\boldsymbol{r},t)$ denote the wave functions of the free-moving ion α. After the collision ($t \to \infty$), the wave functions $\psi_{\alpha n}(\boldsymbol{r},t)$ of the free-moving ion α are given by

$$\psi_{\alpha n}(\boldsymbol{r},t) = e^{-iE_{\alpha n}t} s_\alpha(\boldsymbol{r}) \psi^0_{\alpha n}(\boldsymbol{r} - \boldsymbol{R}_\alpha), \tag{50}$$

where $\psi^0_{\alpha n}(\boldsymbol{r})$ are the stationary Dirac wave functions of ion α at the rest and $s_\alpha(\boldsymbol{r})$ is the translation factor. For low-energy collisions the translation factor and the energy $E_{\alpha n}$ of the moving ion can be taken in the nonrelativistic approximation

$$s_\alpha(\boldsymbol{r}) = \exp(i\boldsymbol{v}_\alpha \cdot \boldsymbol{r}), \quad E_{\alpha n} = \varepsilon_{\alpha n} + v^2_\alpha/2. \tag{51}$$

In general, the plane-wave translation factor is introduced in the basis functions [77] to provide the correct asymptotic behavior at the large internuclear distance R and to improve the convergence of the time-dependent wave function expansion. We did not include the translation factor $s_\alpha(\boldsymbol{r})$ in the basis functions because of the computational complexity of the two-center integral calculations. However, at asymptotic time $t \to \infty$ we can project basis functions $\varphi_{\alpha n}$ onto the space spanned by the basis of the moving ("traveling") orbitals $s_\alpha\varphi_{\alpha n}$. The projected functions form a nonorthonormal basis. We can orthogonalize this basis using the symmetric Löwdin orthogonalization procedure [78], which possesses a remarkable feature: the Löwdin basis is least distorted from the original one in the least-squares sense [79]. As a result, for the large internuclear distance we can obtain the expansion of the time-dependent wave function $\Psi(\boldsymbol{r},t)$ over the basis of the traveling orbitals (for details, see Appendix B),

$$\Psi(\boldsymbol{r},t) \simeq \sum_{\alpha,n} \overline{C}_{\alpha n}(t) e^{i\boldsymbol{v}_\alpha\cdot\boldsymbol{r}} \varphi_{\alpha n}(\boldsymbol{r}),$$
$$\overline{C}_{\alpha n}(t) = \sum_{n'} \overline{K}_{\alpha n,\alpha n'} C_{\alpha n'}(t). \tag{52}$$

The matrix $\overline{K}$ is defined by

$$\overline{K} = KN^{-1/2}, \qquad N = (K^+K),$$
$$K_{\alpha' n',\alpha n} = \delta_{\alpha,\alpha'} \langle \varphi_{\alpha n'}|e^{-i\boldsymbol{v}_\alpha\cdot\boldsymbol{r}}|\varphi_{\alpha n}\rangle. \tag{53}$$

Since the matrix $\overline{K}$ is unitary, the set of coefficients $\overline{C}_{\alpha n}(t)$ is normalized to unity:

$$\sum_{\alpha,n} |\overline{C}_{\alpha n}(t)|^2 = \sum_{\alpha,n} |C_{\alpha n}(t)|^2 = 1, \quad t \to \infty. \tag{54}$$

It should be noted that the error introduced by the expansion (52) is equal to zero, if the basis $\varphi_{\alpha n}$ is complete.

For the transition amplitude $T_{\alpha n}(t)$ we obtain ($t \to \infty$)

$$T_{\alpha n}(t) = \langle \psi_{\alpha n}(\boldsymbol{r},t)|\Psi(\boldsymbol{r},t)\rangle = \sum_{n'} \overline{C}_{\alpha n'}(t) e^{iE_{\alpha n}t} \langle \psi^0_{\alpha n}|\varphi_{\alpha n'}\rangle. \tag{55}$$

The stationary Dirac wave functions $\psi^0_{\alpha n}$, including wave functions of the positive and negative energy spectra, form a complete basis set. Therefore,

$$\sum_{\alpha,n} |T_{\alpha n}|^2 = \sum_{\alpha,n} |\overline{C}_{\alpha n}(t)|^2 = 1. \tag{56}$$

The effectiveness of the projection procedure described in this section (see also Appendix B) can be demonstrated by a simple example of the collision of one-electron ions with bare nuclei $[A^{(Z-1)+}(1s)\text{-}A^{Z+}]$ for the large impact parameters. Let us consider a very short basis $(\varphi_{A,1s},\varphi_{B,1s})$, which contains only one $1s$ function at each center. We suppose that the basis functions of the different centers do not overlap for large values of the impact parameter b and that b is not large enough to neglect the Coulomb interaction between the different ions. In this case the trivial solution of Eqs. (8) and (17) gives us only one nonzero coefficient $|C_{A,1s}| = 1$. Then, the time-dependent wave function $\Psi(\boldsymbol{r},t)$ has a wrong behavior and leads to the nonvanishing probability of the direct excitation and ionization channels, especially for large values of the target velocities. If we use the projected basis and the expansion (52), we also obtain one nonzero coefficient $|\overline{C}_{A,1s}| = 1$, but the correct behavior of the wave function $\Psi(\boldsymbol{r},t)$, which is described by one traveling $1s$ orbital of ion A.

2. Transition probabilities

Transition probabilities $W_{\alpha n}(t)$ are defined by

$$W_{\alpha n}(t) = |T_{\alpha n}(t)|^2. \tag{57}$$

The probability $W_{\alpha n}(t)$, defined by Eqs. (57) and (55), has an oscillatory behavior at $t \to \infty$, because the basis functions $\varphi_{\alpha,n}$ are not the solutions of the hydrogenlike Dirac equation and the basis set is truncated. We can remove the oscillatory component of the probability $W_{\alpha n}(t)$ for the large time $(t \to \infty)$ in the same way, as was done in Refs. [7,8].

At asymptotic time $(t \to \infty)$ the coefficients $C_j^L(t)$ coincide with the coefficients $C_j(t)$. Therefore, the coefficients $C_j(t)$ are the solutions of Eq. (17):

$$i\frac{d\boldsymbol{C}(t)}{dt} = M(t)\boldsymbol{C}(t). \tag{58}$$

Then for the coefficients $\overline{C}_j(t)$ we obtain the equation

$$i\frac{d\overline{\boldsymbol{C}}(t)}{dt} = \overline{K}M(t)\overline{K}^{+}\overline{\boldsymbol{C}}(t). \tag{59}$$

Using the diagonalization procedure for the Hermitian matrix $\overline{K}M\overline{K}^{+}$, we can decompose

$$\overline{K}M\overline{K}^{+} = V\Omega V^{+}, \tag{60}$$

where Ω is a diagonal matrix with eigenvalues $\Omega_{kk} = \omega_k$ and V is a unitary matrix.

We introduce new coefficients $\boldsymbol{B}(t)$ by

$$B_k(t) = [e^{i\Omega t}V^{+}\overline{\boldsymbol{C}}(t)]_k = e^{i\omega_k t}\sum_j V_{jk}^{*}\overline{C}_j(t),$$
$$\sum_k |B_k(t)|^2 = 1. \tag{61}$$

These coefficients have well defined limits at $t \to \infty$. The amplitudes $T_{\alpha n}(t)$, defined by Eq. (55), expressed in terms of the coefficients $\boldsymbol{B}(t)$ read

$$T_j(t) = \sum_{k,l} e^{i(E_j-\omega_k)t}V_{lk}B_k(t)\langle\psi_j^0|\varphi_l\rangle. \tag{62}$$

The for the probabilities $W_j(t)$ we obtain

$$W_j(t) = |T_j(t)|^2 = \sum_k |B_k(t)|^2\left|\sum_l V_{lk}\langle\psi_j^0|\varphi_l\rangle\right|^2 + (\text{oscillating term}). \tag{63}$$

Disregarding the oscillating term [8], we can introduce probabilities $W'_j(t)$ defined as

$$W'_j(t) = \sum_k |B_k(t)|^2\left|\sum_l V_{lk}\langle\psi_j^0|\varphi_l\rangle\right|^2. \tag{64}$$

Since hydrogenlike Dirac wave functions $\psi^0_{\alpha,n}$ of each center α (including the positive and negative Dirac continuum spectra) form a complete basis set, we get

$$\sum_{j\in\alpha}|W'_j(t)|^2 = \sum_k |B_k(t)|^2\sum_l |V_{kl}|^2 = \sum_k |B_k(t)|^2 = 1. \tag{65}$$

The coefficients $B_k(t)$ and the matrix elements have well-defined limits for $t \to \infty$; therefore, also the limit

$$P_{\alpha,n} = \lim_{t\to\infty} W'_{\alpha n}(t) \tag{66}$$

exists. The direct $(P_{\rm d})$, charge transfer $(P_{\rm ct})$, and ionization $(P_{\rm ion})$ probabilities are given by

$$P_{\rm d} = \sum_n{}' P_{A,n}, \qquad P_{\rm ct} = \sum_n{}' P_{B,n},$$
$$P_{\rm ion} = 1 - \sum_{\alpha,n}{}' P_{\alpha n} = 1 - P_{\rm d} - P_{\rm ct}, \tag{67}$$

where the prime at the sum symbol indicates that the summation runs over the discrete bound states of the ion α.

The cross sections for charge-transfer $(\sigma_{\rm ct})$ and ionization $(\sigma_{\rm ion})$ processes are then obtained as usual by integrating the probabilities over the impact parameter b:

$$\sigma_{\rm ct} = 2\pi\int_0^\infty dbbP_{\rm ct}(b), \quad \sigma_{\rm ion} = 2\pi\int_0^\infty dbbP_{\rm ion}(b). \tag{68}$$

3. Z scaling

It is well-known that in the nonrelativistic theory the scale transformation $\boldsymbol{r}' = Z\boldsymbol{r}$ and $\boldsymbol{R}' = Z\boldsymbol{R}$ allows one to transform the wave functions $\psi(\boldsymbol{r})$ and the energies ε of a homonuclear one-electron quasimolecule in the Coulomb field of a nuclear point charge $Z > 1$ to the wave functions $\psi'(\boldsymbol{r}) = Z^{-3/2}\psi(Z\boldsymbol{r})$ and energies $\varepsilon' = \varepsilon/Z^2$ of the H_2^+ molecule. The same scale transformation can be considered in nonrelativistic homonuclear collisions.

The time-dependent Schrödinger equation describing $A^{(Z-1)+}$-A^{Z+} collision is given by

$$\left(-\frac{1}{2}\Delta + \frac{Z}{|\boldsymbol{r}-\boldsymbol{R}_A(t)|} + \frac{Z}{|\boldsymbol{r}-\boldsymbol{R}_B(t)|}\right)\Psi(\boldsymbol{r},t) = i\frac{\partial}{\partial t}\Psi(\boldsymbol{r},t). \tag{69}$$

If in Eq. (69) we set $\boldsymbol{r}' = Z\boldsymbol{r}$, $t' = Z^2t$, and $\boldsymbol{R}'_\alpha(t') = Z\boldsymbol{R}_\alpha(t)$, we obtain the time-dependent Schrödinger equation for the H^+-H collision [4,19]:

$$\left(-\frac{1}{2}\Delta' + \frac{1}{|\boldsymbol{r}'-\boldsymbol{R}'_A(t')|} + \frac{1}{|\boldsymbol{r}'-\boldsymbol{R}'_B(t')|}\right)\Psi(\boldsymbol{r}',t') = i\frac{\partial}{\partial t'}\Psi(\boldsymbol{r}',t'). \tag{70}$$

It should be noted that the scaling $R' = ZR(t)$ holds exactly for a straight-line trajectory. In this case the impact parameter b, the velocity v_α, and projectile energy E are transformed by

$$b' = Zb, \quad v'_\alpha = v_\alpha/Z, \quad E' = E/Z^2. \tag{71}$$

It follows that in symmetric collision systems involving nuclei of charge Z, the probability $P_{\alpha,n}(Z,b,E)$ and the cross section $\sigma_{\alpha,n}(Z,E)$ for any process under consideration can be obtained from the probability $P_{\alpha,n}(1,b',E')$ and the cross section $\sigma_{\alpha,n}(1,E')$ for the same process in the H(1s)-H^+ system by means of the relations

$$P_{\alpha,n}(Z,b,E) = P_{\alpha,n}(1,bZ,E/Z^2),$$
$$\sigma_{\alpha,n}(Z,E) = \frac{1}{Z^2}\sigma_{\alpha,n}(1,E/Z^2). \tag{72}$$

It should be noted that this scaling law is not valid in a relativistic treatment of collisions.

III. RESULTS

A. The choice of the basis

In our relativistic calculations, we used two Dirac-Sturm bases of different size. Both bases include functions of the positive-energy Dirac spectrum and Sturm orbitals corresponding to the negative-energy Dirac spectrum. It should be noted that the constructed bases satisfy the dual kinetic balance conditions [80] and do not contain so-called "spurious" states [81].

The positive-energy functions of the first basis (Basis 1) on each center in the standard nonrelativistic notations of atomic shells are given by $1s$-$3s$, $2p$, $3p$, $3d$, $\overline{4s}$-$\overline{6s}$, $\overline{4p}$-$\overline{6p}$, $\overline{4d}$-$\overline{6d}$, $\overline{4f}$,$\overline{5f}$. Here the overline symbol $(\overline{nl})$ is used to indicate the Dirac-Sturm (pseudostate) basis functions. The total number of positive-energy orbitals of both centers is 220 and the total size of Basis 1, including negative-energy orbitals, is 440. Basis 1 is used for expanding both stationary and time-dependent wave functions.

The basis size can be increased in the calculations of the stationary states of quasimolecules. Positive-energy functions of the second basis (Basis 2) is constructed from 26 atomic shells: $1s$, $\overline{2s}$-$\overline{8s}$, $\overline{2p}$-$\overline{8p}$, $\overline{3d}$-$\overline{8d}$ $\overline{4f}$-$\overline{6f}$ $\overline{5g}$, $\overline{6g}$. In Basis 2, the total number of orbitals of both ions, including the negative-energy spectrum, is equal to 784. This basis is used only in the calculations of the stationary quasimolecular states.

B. Stationary ground states of some homonuclear quasimolecules

1. Energies of the ground state of some homonuclear quasimolecules

In Table I we present the results of our relativistic calculations of the $1\sigma_g$ state energy of the $H_2{}^+$, $Th_2{}^{179+}$, and $U_2{}^{183+}$ quasimolecules for the so-called chemical distance $R = 2/Z$ a.u.. Since the quasimolecule $Th_2{}^{179+}$ was considered as a reference system for testing relativistic effects, it was calculated in a number of articles using high-precision large-scale methods (see, e.g., Refs. [59,82–84]). As one can seen from Table I, there is a good agreement of our data with very accurate values obtained in Refs. [58,59]. The relative precision of our results for the quasimolecules $H_2{}^+$ and $Th_2{}^{179+}$ is increased by an order of magnitude when Basis 1 is replaced with Basis 2.

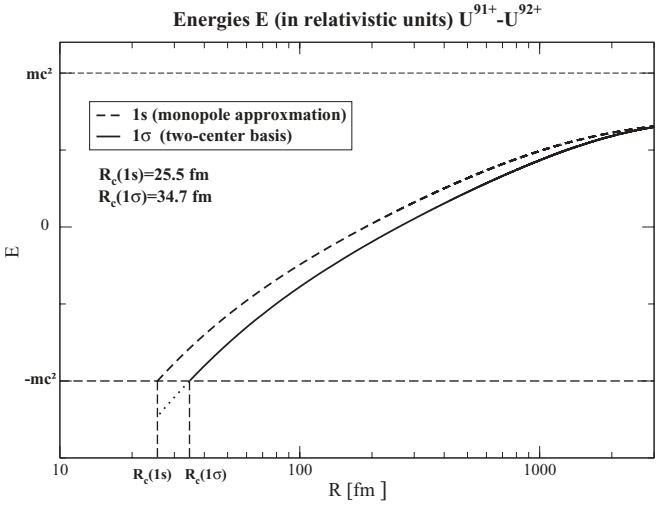

FIG. 3. The $1\sigma_g$ state energy of the U_2 quasimolecule as a function of the internuclear distance R on a logarithmic scale.

In Fig. 3 we display the energy of the $1\sigma_g$ state of the $U_2{}^{183+}$ quasimolecule as a function of the internuclear distance R on a logarithmic scale. In this figure the solid line indicates the energy $E(R)$ calculated using the two-center Dirac-Sturm Basis 2. The dashed line represents the results of the one-center calculations in the monopole approximation. As one can see from Fig. 3, in the two-center basis the $1\sigma_g$ electron "dives" into the negative-energy Dirac continuum at a critical distance $R_c = 34.7$ fm. The critical distance deduced within our type of monopole approximation amounts to $R_c = 25.5$ fm, which is too far from the exact value. It should be noted that in our one-center monopole approximation the basis was centered at the position of the nucleus (A or B) but not at the center of mass located at half of the internuclear distance R, as was done in Refs. [41,62,85]. The monopole approximation used in Ref. [41] is more suitable for the short-distance regime and yields $R_c = 35$ fm for the value of the critical distance.

2. Critical distance

In Table II we present our results for the critical distance R_c in the homonuclear one-electron quasimolecular system $A_2^{(2Z-1)+}$ obtained from our relativistic two-center calculations (Basis 2) and compare them with the corresponding values obtained by other authors. There exists a discrepancy of about 5%–10% between the critical distance data for the point nuclei [27,41,60,61,86,87]. Our results for this case are in a very good

TABLE I. Relativistic energies (a.u.) of the $1\sigma_g$ state of quasimolecules for the point-charge nuclei and $R = 2/Z$ a.u..

	$H_2{}^+$ $(Z = 1)$		$Th_2{}^{179+}$ $(Z = 90)$		$U_2{}^{183+}$ $(Z = 92)$
	$\varepsilon_{1\sigma_+}$	Rel. error	$\varepsilon_{1\sigma_+}$	Rel. error	$\varepsilon_{1\sigma_+}$
Basis 1	−1.102 624 8	1.5×10^{-5}	−9504.573	1.9×10^{-5}	−9965.190
Basis 2	−1.102 640 5	1.0×10^{-6}	−9504.732	2.5×10^{-6}	−9965.307
Others	−1.102 641 6[a]		−9504.756[b]		

[a]Reference [58].
[b]Reference [59].

TABLE II. Critical distances R_c (fm) for homonuclear one-electron quasimolecules $A_2^{(2Z-1)+}$.

	Point nucleus		Extended nucleus		
Z	This work	Others	$\langle R_n^2\rangle^{1/2}$ (fm)	This work	Others
88	24.27	24.24[a]	5.5705	19.91	19.4[c]
90	30.96	30.96[a]	5.7210	27.05	26.5[c]
92	38.43	38.42[a]	5.8569	34.72	34.3[c]
		36.8[b]			34.7[d]
94	46.58	46.57[a]	5.794	43.16	42.6[c]
96	55.38	55.37[a]	5.816	52.09	51.6[c]
98	64.79	64.79[a]	5.844	61.63	61.0[c]
					61.1[d]

[a]Reference [60].
[b]Reference [27].
[c]Reference [63].
[d]Reference [62].

agreement with the results of Ref. [60]. In our calculations for extended nuclei, the finite nuclear size was taken into account using the Fermi model of the nuclear charge distribution (for details, see, e.g., Ref. [88]). The root-mean-square nuclear charge radii $\langle R_n^2\rangle^{1/2}$ were taken from Refs. [89] (for $Z = 88$), [90] (for $Z = 90$), [91] (for $Z = 92$), and [92] (for $Z = 94$, 96,98). In contrast to the point nucleus case, which was frequently considered, only a very small number of works account for the finite nuclear size effect. We can systematically compare our results only with the data obtained in Ref. [63]. The discrepancy between our data and those from Ref. [63] is considerably larger for the extended nuclei than for the pointlike nuclei. A possible reason for that could consist of a rather crude estimate of the nuclear size effect in Ref. [63]. It should also be noted that in the work [63] other values of the nuclear radii, namely, $\langle R_n^2\rangle^{1/2} = \sqrt{3/5}\,1.2\,(2.6\,Z)^{1/3}$ were used. Our calculations showed, however, that the usage of the nuclear radii from Ref. [63] changes the values of R_c by not more than 0.02 fm.

C. Charge-transfer probabilities and cross sections

1. *H(1s)-H$^+$ collisions*

Figure 4 depicts the charge-transfer probabilities $P_{ct}(b)$ for the H(1s)-H$^+$ collision as functions of the impact parameter b for the projectile energies of 2 and 5 keV, respectively. The results of our relativistic calculations for 2 keV (solid line) and 5 keV (dashed line) are found to be very close to nonrelativistic calculations based on the two-center atomic-orbital (AO) expansion [5,93]. This is not surprising, since the relativistic effects are negligible for the H(1s)-H$^+$ collision. Our calculations were performed for the projectile moving on a straight-line trajectory which corresponds to full screening of the target nuclear charge by the 1s electron.

As was demonstrated in Ref. [5], the two-center AO expansion data are in a very good agreement with results obtained by a direct numerical solution of the nonrelativistic Schrödinger equation [14]. In the review [5], the two-center AO expansion data [93] are also compared with the results [94,95], obtained by the expansion with respect to the

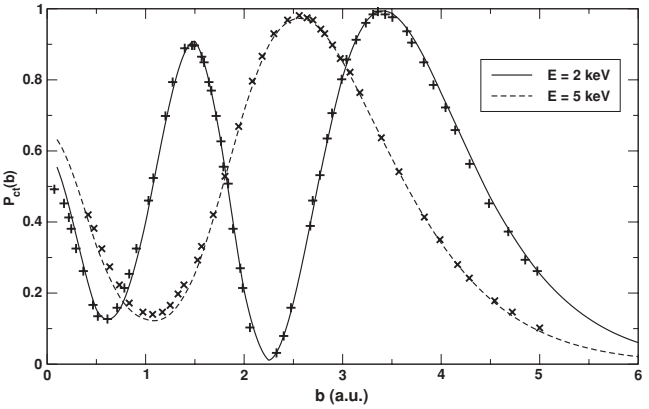

FIG. 4. Charge-transfer probabilities $P_{ct}(b)$ for the H(1s)-H$^+$ collision as functions of the impact parameter b. Our results for the projectile energies 2 keV (solid line) and 5 keV (dashed line) are compared to the related results from the AO-expansion calculations [5,93] (symbols "+" and "×").

"nonmoving" Hylleraas basis functions. It should be noted that the Hylleraas expansion data are similar to the results of Refs. [14,93] and to our results in trend but differ in both phase and magnitude.

In Table III we present the total charge-transfer cross sections σ_{ct} in H(1s)-H$^+$ collisions for a wide range of projectile energies (from 0.5 to 100 keV) and compare them with nonrelativistic large-scale calculations of a recent article [13], which can be considered as an extension of the pioneering works [8,96], where the analytical Sturmian basis set expansion was used. We also give the cross-section values, deduced from the experimental results [97]. The relative uncertainties of the recommended and interpolated experimental data are about 5%–10%. As one can see from Table III, our results are

TABLE III. Charge-transfer cross section σ_{ct} for the H(1s)-H$^+$ collision, in units of 10^{-17} cm^2.

Projectile energy E (keV)	$\sigma_{ct}(E)$ This work	$\sigma_{ct}(E)$ Winter [13]	$\sigma_{ct}(E)$ Expt.[a]
0.5	199.6		
0.7	186.9		
1.0	172.4	173.0	171
2.0	144.9		144
4.0	117.5	118.1	115[b]
5.0	107.8		110
10.0	81.3		77.5
15.0	63.5	67.41	55.6[b]
20.0	48.9		44.5
25.0	36.2	39.45	35.3[b]
30.0	26.6		27.6[b]
40.0	15.3		16.5[b]
50.0	9.1	10.04	9.9
60.0	5.6		5.9[b]
70.0	3.5		3.6[b]
80.0	2.3		2.3[b]
100.0	1.1	1.11	1.1

[a]Recommended values [97] deduced from the experimental data.
[b]Interpolated values obtained using an analytical fitting function [97].

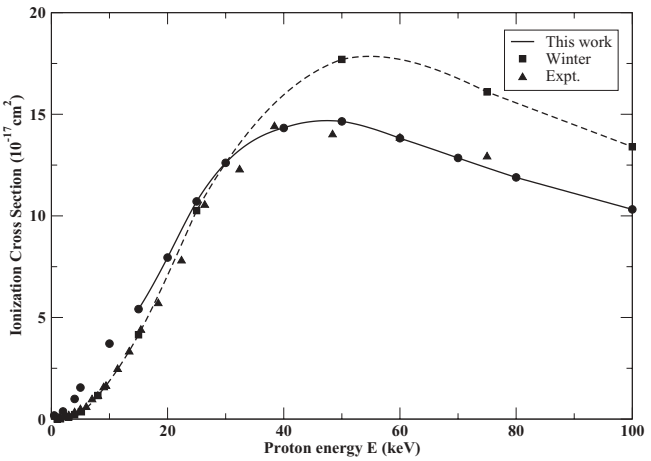

FIG. 5. Ionization cross section $\sigma_{\rm ion}(E)$ for the H($1s$)-H$^+$ collision as a function of the projectile energy E. The solid line is obtained by the interpolation of our results indicated by circles, the dashed line is obtained by the interpolation of data from Ref. [13], and the triangles indicate the experimental data from Refs. [98,99].

in a good agreement with the theoretical data of Ref. [13] and with the experimental data.

The ionization cross sections, computed in this work according to Eqs. (67) and (68), are displayed in Fig. 5. Our results are in a good agreement with the experimental data within the range of the proton energy from 20 to 80 keV. At energies less than 15 keV we observe a significant relative deviation of our results from the experimental data. This is probably due to the fact that the absolute uncertainty of our data is approximately the same in the whole region of the energies [about $(1–3)\times10^{-17}$ cm^2], while at low energies the ionization cross section tends to zero. This leads to a large relative error in the low-energy region.

In contrast to our results, the theoretical data of Ref. [13], which are shown in Fig. 5 by squares, are in a good agreement with the experimental data in the low-energy region (less than 25 keV) and differ significantly (at least by 25%) from the experimental data for energies larger than 40 keV. The reason of this discrepancy is unclear to us.

2. $Ne^{9+}(1s)$-Ne^{10+} collisions

To study the role of the relativistic effects in the homonuclear collisions and to test our approach we calculated the charge transfer cross sections for the Ne^{9+}($1s$)-Ne^{10+} collisions with the standard value of the speed of light ($c = 137.036$ a.u.) and in the nonrelativistic limit ($c \to \infty$) by multiplying the standard value of the speed of light by the factor 1000. The obtained values are presented in Table IV. It should be noted that the projectile energy values are divided by Z^2 (Z is the nuclear charge) and the values of the charge-transfer cross section $\sigma_{\rm ct}$ are multiplied by the factor Z^2. This was done in order to compare the Ne^{9+}($1s$)-Ne^{10+} cross-section data with the H($1s$)-H$^+$ results in accordance with the scaling law (72). As one can see from the table, the relativistic effects, which decrease the values of the charge-transfer cross section, are rather small and can be estimated as 0.5–0.8 $(\alpha Z)^2$, where α is the fine-structure constant. In Table IV, we also compare our scaled nonrelativistic Ne^{9+}($1s$)-Ne^{10+} data with the H($1s$)-H$^+$ results. It should be noted that our calculations for the Ne^{9+}($1s$)-Ne^{10+} collision were performed for the Rutherford trajectory (see Sec. II A 2). This is probably the reason for a very small discrepancy between the data presented in the third and fourth columns of Table IV.

TABLE IV. Charge-transfer cross section $\sigma_{\rm ct}(E)$ (10^{-17} cm^2) as a function of the projectile energy E for Ne^{9+}($1s$)-Ne^{10+} ($Z = 10$) and H($1s$)-H$^+$ collisions.

	Ne^{9+}($1s$)-Ne^{10+}		H($1s$)-H$^+$	Ne^{9+}($1s$)-Ne^{10+}
E/Z^2 (keV/u)	$\sigma_{\rm ct}(E)Z^2$ Rel.[a]	$\sigma_{\rm ct}(E)Z^2$ Nonrel.[b]	$\sigma_{\rm ct}(E)$	$\sigma_{\rm ct}(E)Z^2$ Born approximation[c]
1.0	171.6	172.2	172.4	188.4
2.0	144.3	144.8	144.9	150.7
4.0	117.1	117.5	117.5	114.8
5.0	107.3	107.7	107.8	107.3
10.0	80.8	81.3	81.3	76.2
15.0	63.0	63.5	63.5	57.6
20.0	48.5	48.9	48.9	48.2
25.0	35.9	36.2	36.2	38.1
30.0	26.4	26.7	26.6	30.1
40.0	15.1	15.3	15.3	19.9
50.0	9.0	9.1	9.1	13.7
60.0	5.6	5.6	5.6	9.1
70.0	3.5	3.5	3.5	5.4
80.0	2.3	2.3	2.3	3.6
100.0	1.1	1.1	1.1	2.0

[a]Relativistic calculations.
[b]Nonrelativistic limit ($c \to \infty$).
[c]Born approximation [100].

It is also of interest to compare our results with the calculations performed within the plane-wave Born (PWB) approximation. The results of such a calculation for the Ne^{9+}($1s$)-Ne^{10+} collision [100] are presented in the fifth column of Table IV. The details of the modified PWB method can be found in Ref. [101]. It is seen from the table that the PWB data are in a reasonable agreement with the more elaborated calculation.

3. $Xe^{53+}(1s)$-Xe^{54+} collisions

The relativistic effect for the Xe^{53+}($1s$)-Xe^{54+} collisions is considerably larger than for the Ne^{9+}($1s$)-Ne^{10+} collisions. The computed relativistic (solid line) and nonrelativistic (dashed line) charge transfer probabilities $P_{\rm ct}(b)$ as functions of the impact parameter b for the projectile energy of 5.9 MeV/u are displayed in Fig. 6. The oscillatory behavior of both curves is the same but the nonrelativistic curve is shifted toward higher impact parameters.

In Table V we present the relativistic and nonrelativistic values of the charge-transfer cross section for the Xe^{53+}($1s$)-Xe^{54+} collision scaled to $Z = 1$. As can be seen from the table, the relativistic effect increases from 10% to 40% with increasing the projectile energy.

4. $U^{91+}(1s)$-U^{92+} collisions

The calculations of the charge-transfer probabilities and cross sections for the U^{91+}($1s$)-U^{92+} collisions were

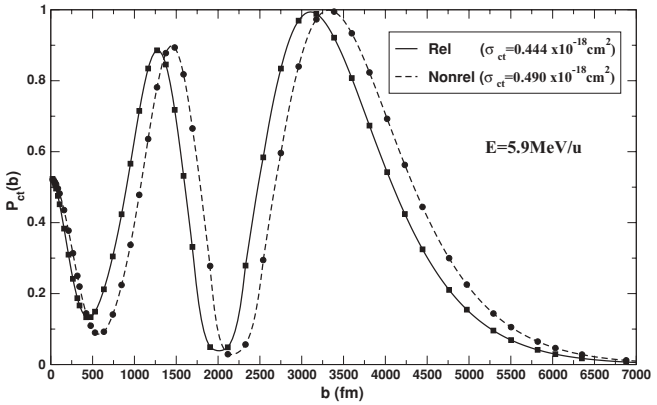

FIG. 6. The charge-transfer probability $P_{ct}(b)$ for $Xe^{53+}(1s)$-Xe^{54+} collision as a function of the impact parameter b. The solid line interpolates the relativistic values (squares) and the dashed line corresponds to the nonrelativistic limit. In both cases, the projectile energy is $E = 5.9$ MeV/u.

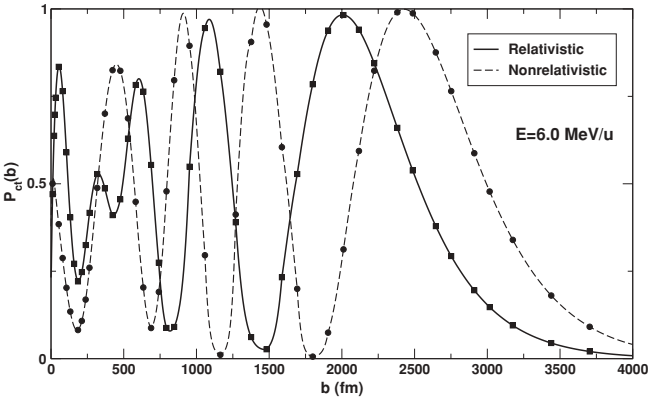

FIG. 7. Charge-transfer probability $P_{ct}(b)$ for the $U^{91+}(1s)$-U^{92+} collision as a function of the impact parameter b. The solid line interpolates the relativistic values (squares) and the dashed line corresponds to the nonrelativistic limit. In both cases, the projectile energy is $E = 6.0$ MeV/u.

performed for extended nuclei. The Fermi model of the nuclear charge distribution with $R_{nucl} = 5.8569$ fm was used as in [91].

The computed relativistic (squares) and nonrelativistic values (circles) for the charge-transfer probabilities $P_{ct}(b)$ together with the interpolating curves are displayed in Fig. 7. It is seen from the figure that the nonrelativistic and relativistic probabilities significantly differ. The nonrelativistic curve (dashed line) is shifted toward higher impact parameters compared to the relativistic one (solid line).

The same curves as in Fig. 7 but in the small impact parameter region (0–200 fm) are shown in Fig. 8. This figure demonstrates the difference between the relativistic and nonrelativistic charge-transfer probabilities in the critical and supercritical regions of the impact parameter b. In Fig. 8, the vertical dashed line indicates the critical impact parameter $b_c = 27.5$ fm. For $b = b_c$ the $1\sigma_g$ ground-state level of the $U_2{}^{193+}$ quasimolecule reaches the negative-energy Dirac continuum. It should be noted that for the non-straight-line (Rutherford) trajectory the value of the critical impact parameter b_c is less than the critical distance R_c presented in Table II. For values of b smaller than b_c, the $1\sigma_g$ level dives into the negative-energy continuum.

In Table VI we present the results of our relativistic (third column) and nonrelativistic (fourth column) calculations of the total charge-transfer cross section $\sigma_{ct}(E)$, scaled to $Z = 1$, for the $U^{91+}(1s)$-U^{92+} collision at different projectile energies E. The values of $\sigma_{ct}(E)$ were obtained for target and projectile ions moving on the Rutherford trajectories. As one can see from the table, the relativistic effect amounts to about 30% of the nonrelativistic value of σ_{ct}. In the fifth column of Table VI, we also present our results obtained for for the projectile ion moving along a straight-line trajectory (in this case the target ion is assumed to be at rest). As one can see from the table, the difference between the results obtained for the straight-line trajectory and the Rutherford one is very small. The nonrelativistic values of the charge-transfer cross section for the $U^{91+}(1s)$-U^{92+} collision, scaled to $Z = 1$, are also compared with the cross section $\sigma_{ct}(E)$ for the $H(1s)$-H^+ collision, presented in the sixth column of Table VI.

TABLE V. Charge-transfer cross section $\sigma_{ct}(E)$ (10^{-17} cm^2) as a function of the projectile energy E for $Xe^{9+}(1s)$-Xe^{10+} and $H(1s)$-H^+ collisions.

	$Xe^{53+}(1s)$-Xe^{54+} ($Z = 54$)			$H(1s)$-H^+ ($Z = 1$)
E/Z^2 (keV/u)	E (MeV/u)	$\sigma_{ct}(E)Z^2$ Rel.[a]	$\sigma_{ct}(E)Z^2$ Nonrel.[b]	$\sigma_{ct}(E)$
1.234 57	3.6	148.3	163.3	165.0
2.023 32	5.9	129.4	143.0	144.9
3.429 36	10.0	109.1	123.8	124.8
34.2936	100.0	13.3	20.6	20.7

[a]Relativistic calculations.

[b]Nonrelativistic limit ($c \to \infty$).

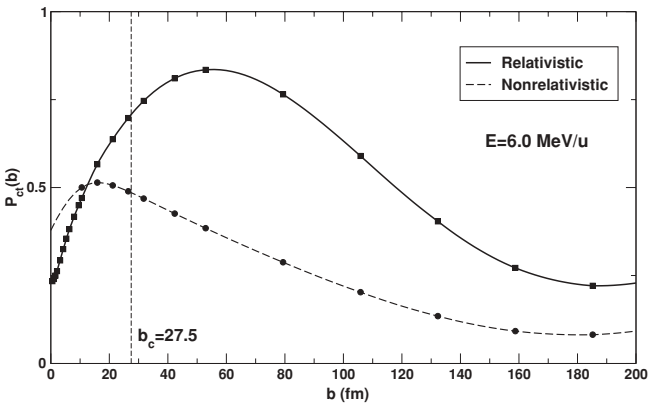

FIG. 8. Charge-transfer probability $P_{ct}(b)$ for the $U^{91+}(1s)$-U^{92+} collision as a function of the impact parameter b in the small b region. The value $b = b_c$ corresponds to the diving of the $1\sigma_g$ level into the negative-energy Dirac continuum. The solid line interpolates the relativistic values while the dashed line corresponds to the nonrelativistic limit.

TABLE VI. Charge-transfer cross section $\sigma_{ct}(E)$ (10^{-17} cm^2) as a function of the projectile energy E for the $U^{91+}(1s)$-U^{92+} and $H(1s)$-H^+ collisions.

	$U^{91+}(1s)$-U^{92+}				$H(1s)$-H^+
Energy E/Z^2 (keV/u)	Energy E (MeV/u)	$\sigma_{ct}Z^2$ Rel.	$\sigma_{ct}Z^2$ Nonrel.	$\sigma_{ct}Z^2$ Nonrel. str. line	σ_{ct}
0.708 89	6.0	135.3	184.2	185.0	186.4
0.767 96	6.5	132.7	181.3	182.0	183.1
0.827 03	7.0	130.3	178.2	179.1	180.1
1.181 47	10.0	117.1	165.8	166.7	167.6

IV. CONCLUSION

In this article we presented a method for relativistic calculations of one-electron two-center quasimolecular system in both stationary and time-dependent regimes. The method is suitable for a wide range of internuclear distances including the critical regime, when the ground state of the quasimolecule can dive into the negative-energy Dirac continuum. Using this method we calculated the energies of the H_2, Th_2^{179+}, and U_2^{183+} quasimolecules, the critical distances for some homonuclear quasimolecules $A^{+(2Z-1)}$ ($Z = 88,90,92,94,96,98$), and the charge transfer probabilities, charge transfer, and ionization cross sections in $H(1s)$-H^+, $Ne^{9+}(1s)$-Ne^{10+}, $Xe^{53+}(1s)$-Xe^{54+}, and $U^{91+}(1s)$-U^{92+} low-energy collisions.

The results of our calculations of the charge-transfer probabilities and cross sections for the $H(1s)$-H^+ collision are in a good agreement with experimental data and with theoretical results obtained by other authors. The influence of the relativistic effects on the charge-transfer probabilities and cross sections for the $Ne^{9+}(1s)$-Ne^{10+}, $Xe^{53+}(1s)$-Xe^{54+}, and $U^{91+}(1s)$-U^{92+} collisions is investigated. We demonstrated that the relativistic and nonrelativistic charge-transfer probabilities as functions of the impact parameter exhibit the same oscillatory behavior at low energies, but the relativistic curves are shifted toward lower impact parameters compared to the nonrelativistic ones. In the case of the $U^{91+}(1s)$-U^{92+} collision, the relativistic effects reduce the values of the cross section by about 30%.

In further investigations we intend to study in more detail the effect of the diving of the $1\sigma_g$ level of the U_2^{183+} quasimolecule into the negative-energy Dirac spectrum and the influence of this effect on the values of the charge-transfer probability. With this goal, we are going to develop an approach which would allow us to compare the calculated probabilities with and without the diving of the ground state into the negative-energy continuum. We also plan to extend our method to collisions involving many-electron ions and neutral atoms. This will allow us to study the $1s$-$1s$ charge transfer in low-energy heavy ion-atom collisions. Such experiments, which were successfully performed for low-Z collisions many years ago [102–105], are presently under preparation for high-Z collisions at GSI.

ACKNOWLEDGMENTS

We thank V. Shevelko for providing us with his PWB results for the charge-transfer probabilities and for valuable discussions. This work was supported by DFG (Grant No. 436RUS113/950/0-1), by the GSI Helmholtz Zentrum für Schwerionenforschung, by RFBR (Grants No. 08-02-91967 and No. 10-02-00450), by the Ministry of Education and Science of Russian Federation (Program for Development of Scientific Potential of High School, Grant No. 2.1.1/1136; Program "Scientific and Pedagogical Specialists for Innovative Russia," Grant No. P1334), and by the ExtreMe Matter Institute EMMI in the framework of the Helmholtz Alliance HA216/EMMI. Y.S.K. acknowledges financial support by the Dynasty Foundation, DAAD (Programm Ostpartnerschaften), G-RISC (Grant No. P-2010b-5), and FAIR-Russia Research Center. V.M.S. acknowledges financial support from the Alexander von Humboldt Foundation.

APPENDIX A: TWO-CENTER MATRIX ELEMENTS

1. Two-center overlap integrals

Let us consider the two-center overlap integrals $S_{ab}^{(0)}$. We remind the reader that superscript (0) means that the integral is considered in the local coordinate frame, where the z axis is directed along internuclear axis A-B. The integral $S_{ab}^{(0)}$ can be divided into two parts,

$$S_{ab}^{(0)} = \langle a|\, b\rangle = \langle a|\, b\rangle_A + \langle a|\, b\rangle_B, \tag{A1}$$

where the notations $\langle\,\rangle_A$ and $\langle\,\rangle_B$ imply the integration over the regions V_A and V_B, respectively (see Fig. 2). Using the reexpansions of the large and small components onto the center A (in the region V_A) and onto the center B (in the region V_B), we obtain

$$\begin{aligned}\langle a|b\rangle_A &= \delta_{\mu_a,\mu_b}\int_0^\infty dr\big[P_a(r)\overline{p}_{\kappa_a\mu_a}(b|r) + Q_a(r)\overline{q}_{\kappa_a\mu_a}(b|r)\big],\\ \langle a|b\rangle_B &= (-1)^{l_b-l_a}\delta_{\mu_a,\mu_b}\int_0^\infty dr\big[P_b(r)\overline{p}_{\kappa_b\mu_a}(a|r) + Q_b(r)\overline{q}_{\kappa_b\mu_a}(a|r)\big].\end{aligned} \tag{A2}$$

The matrix elements of the nuclear binding potentials, $V^A_{\rm nucl}(r_A)$ and $V^B_{\rm nucl}(r_B)$, and of the mass operator βmc^2 are evaluated similarly as the overlap integral.

2. Two-center gradient matrix elements

As in case of the overlap integral, the region of integration for the gradient matrix element $G^{(0)}_{ab}(q)$ is divided into two parts:

$$G^{(0)}_{ab}(q) = \langle a|\nabla_q|\, b\rangle = \langle a|\nabla_q|b\rangle_A + \langle a|\nabla_q|b\rangle_B. \quad \text{(A3)}$$

Here index $q = 1,0,-1$ enumerates covariant spherical coordinates. Using the Gauss theorem [75] for the integration over region A, we obtain

$$G^{(0)}_{ab}(q) = -\langle b|\nabla_q|a\rangle_A + \langle a|\nabla_q|b\rangle_B + \delta_{q,0}\langle a|b\rangle_S, \quad \text{(A4)}$$

where $\langle a|b\rangle_S$ is the surface integral over the region S (see Fig. 2). The volume integrals over regions A and B are given by

$$\begin{aligned}\langle b|\nabla_q|a\rangle_A &= \sum_\kappa{}' g^{1q}(j\mu_b, j_a\mu_a)\int_0^\infty dr\big[\overline{p}_{\kappa\mu_b}(b|r)\hat{D}_{\kappa,\kappa_a} \\ &\quad\times P_a(r) + \overline{q}_{\kappa\mu_b}(b|r)\hat{D}_{-\kappa,-\kappa_a}Q_a(r)\big], \\ \langle a|\nabla_q|b\rangle_B &= \sum_\kappa{}'(-1)^{l_a-l}g^{1q}(j\mu_a, j_b\mu_b)\int_0^\infty dr\big[\overline{p}_{\kappa\mu_a}(a|r) \\ &\quad\times \hat{D}_{\kappa,\kappa_b}P_b(r) + \overline{q}_{\kappa\mu_a}(a|r)\hat{D}_{-\kappa,-\kappa_b}Q_b(r)\big],\end{aligned} \quad \text{(A5)}$$

where the prime at the sum symbol indicates that the summation is restricted to odd values of $l_a + l$ and $l_b + l$, and the operator $D_{\kappa,\kappa'}$ is defined by

$$D_{\kappa,\kappa'} = \frac{d}{dr} + \frac{\kappa'(\kappa'+1) - \kappa(\kappa+1)}{2r}. \quad \text{(A6)}$$

The coefficients $g^{kq}(j\mu, j'\mu')$ are the relativistic analogs of the Gaunt coefficients [76]

$$\begin{aligned}g^{kq}(j\mu, j'\mu') &= \frac{\sqrt{(2j+1)(2j'+1)}}{2k+1}(-1)^{\frac{1}{2}+\mu'} \\ &\quad\times C^{k0}_{j-\frac{1}{2},j'\frac{1}{2}}C^{kq}_{j\mu,j'-\mu'}.\end{aligned} \quad \text{(A7)}$$

The relativistic Gaunt coefficient is nonzero only if $l + l' + k$ is even.

The surface integral is given by

$$\begin{aligned}\langle a|b\rangle_S = \delta_{\mu_a,\mu_b}\frac{1}{2}\Bigg[&\sum_{m,m_s}C^{j_a\mu_a}_{l_am,\frac{1}{2}m_s}C^{j_b\mu_a}_{l_bm,\frac{1}{2}m_s}\int_{R/2}^\infty dr\frac{1}{r}P_a(r) \\ &\times P_b(r)U_{l_al_bm}(R/2r)\sum_{m,m_s}C^{j_a\mu_a}_{\bar{l}_am,\frac{1}{2}m_s}C^{j_b\mu_a}_{\bar{l}_bm,\frac{1}{2}m_s} \\ &\times\int_{R/2}^\infty dr\frac{1}{r}Q_a(r)Q_b(r)U_{\bar{l}_a\bar{l}_bm}(R/2r)\Bigg],\end{aligned} \quad \text{(A8)}$$

where

$$\begin{aligned}U_{l_al_bm}(x) &= (-1)^{l_b-m}\sqrt{(2l_a+1)(2l_b+1)} \\ &\quad\times K_{l_a|m|}K_{l_b|m|}P^{|m|}_{l_a}(x)P^{|m|}_{l_b}(x).\end{aligned} \quad \text{(A9)}$$

3. Two-center $(\boldsymbol{\alpha}\cdot\boldsymbol{p})$ matrix elements

The two-center $(\boldsymbol{\alpha}\cdot\boldsymbol{p})$ matrix elements $A^{(0)}_{ab}$ can be divided into three parts, similar to the gradient matrix elements $G^{(0)}_{ab}(q)$ in Eq. (A4),

$$\begin{aligned}A^{(0)}_{ab} &= \langle a|\boldsymbol{\alpha}\cdot\boldsymbol{p}|\, b\rangle \\ &= \langle b|\boldsymbol{\alpha}\cdot\boldsymbol{p}|a\rangle_A + \langle a|\boldsymbol{\alpha}\cdot\boldsymbol{p}|b\rangle_B + \frac{1}{i}\langle a|\boldsymbol{\alpha}_0|b\rangle_S,\end{aligned} \quad \text{(A10)}$$

where the volume integrals $\langle b|\boldsymbol{\alpha}\cdot\boldsymbol{p}|a\rangle_A$ and $\langle b|\boldsymbol{\alpha}\cdot\boldsymbol{p}|a\rangle_A$ are given by

$$\begin{aligned}\langle b|\boldsymbol{\alpha}\cdot\boldsymbol{p}|a\rangle_A &= \delta_{\mu_a,\mu_b}\int_0^\infty dr\left[\left(-\frac{dQ_a}{dr} + \frac{\kappa_a Q_a}{r}\right)\right. \\ &\quad\left.\times\,\overline{p}_{\kappa_a\mu_a}(b|r) + \left(\frac{dP_a}{dr} + \frac{\kappa_a P_a}{r}\right)\overline{q}_{\kappa_a\mu_a}(b|r)\right], \\ \langle a|\boldsymbol{\alpha}\cdot\boldsymbol{p}|b\rangle_B &= (-1)^{l_a-l_b}\delta_{\mu_a,\mu_b}\int_0^\infty dr\left[\left(-\frac{dQ_b}{dr} + \frac{\kappa_b Q_b}{r}\right)\right. \\ &\quad\left.\times\,\overline{p}_{\kappa_b\mu_a}(a|r) + \left(\frac{dP_b}{dr} + \frac{\kappa_b P_b}{r}\right)\overline{q}_{\kappa_b\mu_a}(a|r)\right].\end{aligned} \quad \text{(A11)}$$

The last term in Eq. (A10) is the surface integral, which is given by

$$\begin{aligned}\frac{1}{i}\langle a|\boldsymbol{\alpha}_0|b\rangle_S &= \delta_{\mu_a,\mu_b}\sum_{m,m_s}m_s C^{j_a\mu_a}_{\bar{l}_am,\frac{1}{2}m_s}C^{j_b\mu_a}_{l_bm,\frac{1}{2}m_s} \\ &\quad\times\int_{R/2}^\infty dr\frac{1}{r}Q_a(r)P_b(r)U_{\bar{l}_al_bm}(R/2r) \\ &\quad+\delta_{\mu_a,\mu_b}\sum_{m,m_s}m_s C^{j_a\mu_a}_{l_am,\frac{1}{2}m_s}C^{j_b\mu_a}_{\bar{l}_bm,\frac{1}{2}m_s} \\ &\quad\times\int_{R/2}^\infty dr\frac{1}{r}P_a(r)Q_b(r)U_{l_a\bar{l}_bm}(R/2r).\end{aligned} \quad \text{(A12)}$$

APPENDIX B: PROJECTION ONTO THE SPACE OF THE TRAVELING ORBITALS

As is mentioned in Sec. II D, the finite basis expansion

$$\Psi(\boldsymbol{r},t) = \sum_{\alpha,n}C_{\alpha n}(t)\varphi_{\alpha n}(\boldsymbol{r}) \quad \text{(B1)}$$

over the set of functions $\varphi_{\alpha,n}(\boldsymbol{r})$ does not provide the correct asymptotic behavior $(t\to\infty)$ of the time-dependent wave function $\Psi(\boldsymbol{r},t)$. However, we can project the basis functions $\varphi_{\alpha n}$ onto the space spanned by the orthonormal basis of the traveling orbitals $s_\alpha\varphi_{\alpha n}$. The projected basis functions $\varphi^{(p)}_{\alpha n}(\boldsymbol{r})$ for the plane-wave translation factor $s_\alpha(\boldsymbol{r}) = \exp(i\boldsymbol{v}_\alpha\cdot\boldsymbol{r})$ are given by

$$\varphi^{(p)}_{\alpha n}(\boldsymbol{r}) = \sum_{n'}K_{\alpha n',\alpha n}e^{i\boldsymbol{v}_\alpha\cdot\boldsymbol{r}}\varphi_{\alpha n'}(\boldsymbol{r}), \quad \text{(B2)}$$

where the coefficients $K_{\alpha' n',\alpha n}$ are defined as

$$K_{\alpha' n',\alpha n} = \delta_{\alpha,\alpha'}\langle\varphi_{\alpha n'}|e^{-i\boldsymbol{v}_\alpha\cdot\boldsymbol{r}}|\varphi_{\alpha n}\rangle. \quad \text{(B3)}$$

The projected $\varphi_{\alpha n}^{(p)}(\boldsymbol{r})$ basis set is not orthonormal, since the finite basis $\varphi_{\alpha n}$ is incomplete and the matrix K is nonunitary. In particular,

$$\sum_{n'} |K_{\alpha n',\alpha n}|^2 < 1. \tag{B4}$$

We can use the Löwdin orthogonalization procedure [78] to obtain the orthogonal basis set $\overline{\varphi}_{\alpha n}(\boldsymbol{r})$, which is closest to the original nonorthogonal basis $\varphi_{\alpha n}^{(p)}(\boldsymbol{r})$ in the least-squares sense,

$$\overline{\varphi}_{\alpha n} = \sum_{n'} (N^{-1/2})_{\alpha n',\alpha n} \varphi_{\alpha n'}^{(p)}(\boldsymbol{r}), \tag{B5}$$

where the overlap matrix N is given by

$$N_{\alpha n,\alpha n'} = \langle \varphi_{\alpha n}^{(p)} | \varphi_{\alpha n'}^{(p)} \rangle, \quad N = K^+ K. \tag{B6}$$

Then we replace the original basis $\varphi_{\alpha n}$ with the orthonormal basis $\overline{\varphi}_{n\alpha}$ in the time-dependent wave function expansion (B1). As a result, we obtain the expansion of the wave function $\Psi(\boldsymbol{r},t)$ over the basis of the traveling orbitals

$$\Psi(\boldsymbol{r},t) \simeq \sum_{\alpha,n} C_{\alpha n}(t) \overline{\varphi}_{\alpha n}(\boldsymbol{r}) = \sum_{\alpha,n} \overline{C}_{\alpha n}(t) e^{i \boldsymbol{v}_\alpha \cdot \boldsymbol{r}} \varphi_{\alpha n}(\boldsymbol{r}), \tag{B7}$$

where the coefficients $\overline{C}_{\alpha n}$ are defined by

$$C_{\alpha n}(t) = \sum_{n'} \overline{K}_{\alpha n,\alpha n'} C_{\alpha n'}(t), \quad \overline{K} = K N^{-1/2}. \tag{B8}$$

Here matrix $N^{-1/2}$ plays a role of the normalization factor. The renormalized matrix $\overline{K}$ is unitary and the set of new coefficients $\overline{C}_{\alpha n}(t)$ is normalized to unity ($t \to \infty$):

$$\sum_{\alpha,n} |\overline{C}_{\alpha n}(t)|^2 = \sum_{\alpha,n} |C_{\alpha n}(t)|^2 = 1. \tag{B9}$$

[1] O. B. Firsov, Zh. Eksp. Teor. Fiz. **21**, 1001 (1951).
[2] Yu. N. Demkov, Uchen. Zap. Leningr. Univ. **146**, 74 (1952).
[3] D. R. Bates, H. S. W. Massey, and A. L. Stewart, Proc. R. Soc. London A **216**, 437 (1953).
[4] B. H. Bransden and M. R. C. McDowell, *Charge Exchange and the Theory of Ion-Atom Collisions* (Oxford University Press, New York, 1992).
[5] W. Fritsch and C. D. Lin, Phys. Rep. **202**, 1 (1991).
[6] T. G. Winter, Adv. At. Mol. Opt. Phys. **52**, 391 (2005).
[7] D. F. Gallaher and L. Wilets, Phys. Rev. **169**, 139 (1968).
[8] R. Shakeshaft, Phys. Rev. A **14**, 1626 (1976).
[9] J. F. Reading, A. L. Ford, and R. L. Becker, J. Phys. B **14**, 1995 (1981).
[10] W. Fritsch and C. D. Lin, Phys. Rev. A **27**, 3361 (1983).
[11] A. M. Ermolaev, J. Phys. B **23**, L45 (1990).
[12] N. Toshima, Phys. Rev. A **59**, 1981 (1999).
[13] T. G. Winter, Phys. Rev. A **80**, 032701 (2009).
[14] N. Grün, A. Mühlhans, and W. Scheid, J. Phys. B **15**, 4043 (1982).
[15] A. Kolakowska, M. S. Pindzola, F. Robicheaux, D. R. Schultz, and J. C. Wells, Phys. Rev. A **58**, 2872 (1998).
[16] A. Kolakowska, M. S. Pindzola, and D. R. Schultz, Phys. Rev. A **59**, 3588 (1999).
[17] D. R. Schultz, M. R. Strayer, and J. C. Wells, Phys. Rev. Lett. **82**, 3976 (1999).
[18] X.-M. Tong, D. Kato, T. Watanabe, and S. Ohtani, Phys. Rev. A **62**, 052701 (2000).
[19] J. S. Briggs and J. H. Macek, J. Phys. B **6**, 982 (1973); **6**, 2484 (1973).
[20] J. Eichler and W. E. Meyerhof, *Relativistic Atomic Collisions* (Academic Press, New York, 1995).
[21] V. M. Shabaev, Phys. Rep. **356**, 119 (2002).
[22] J. Eichler and T. Stöhlker, Phys. Rep. **439**, 1 (2007).
[23] Y. B. Zeldovich and V. S. Popov, Usp. Fiz. Nauk **105**, 403 (1971) [Sov. Phys. Usp. **14**, 673 (1972)].
[24] J. Rafelski, L. P. Fulcher, and W. Greiner, Phys. Rev. Lett. **27**, 958 (1971).
[25] W. Greiner, B. Müller, and J. Rafelski, *Quantum Electrodynamics of Strong Fields* (Springer-Verlag, Berlin, 1985).
[26] U. Müller-Nehler and G. Soff, Phys. Rep. **246**, 101 (1994).
[27] J. Rafelski and B. Müller, Phys. Lett. B **65**, 205 (1976).
[28] J. Eichler, *Lectures on Ion-Atom Collisions: From Nonrelativistic to Relativistic Collisions* (Elsevier, Amsterdam, 2005).
[29] U. Becker, N. Grün, W. Scheid, and G. Soff, Phys. Rev. Lett. **56**, 2016 (1986).
[30] M. R. Strayer, C. Bottcher, V. E. Oberacker, and A. S. Umar, Phys. Rev. A **41**, 1399 (1990).
[31] J. Thiel, A. Bunker, K. Momberger, N. Grün, and W. Scheid, Phys. Rev. A **46**, 2607 (1992).
[32] K. Momberger, A. Belkacem, and A. H. Sorensen, Phys. Rev. A **53**, 1605 (1996).
[33] J. C. Wells, V. E. Oberacker, M. R. Strayer, and A. S. Umar, Phys. Rev. A **53**, 1498 (1996).
[34] D. C. Ionescu and A. Belkacem, Phys. Scr. T **80**, 128 (1999).
[35] M. S. Pindzola, Phys. Rev. A **62**, 032707 (2000).
[36] O. Busic, N. Grün, and W. Scheid, Phys. Rev. A **70**, 062707 (2004).
[37] J. Eichler, Phys. Rep. **193**, 165 (1990).
[38] K. Rumrich, G. Soff, and W. Greiner, Phys. Rev. A **47**, 215 (1993).
[39] K. Momberger, N. Grün, and W. Scheid, J. Phys. B **26**, 1851 (1993).
[40] M. Gail, N. Grün, and W. Scheid, J. Phys. B **36**, 1397 (2003).
[41] G. Soff, J. Reinhardt, and W. Betz, Phys. Scr. **17**, 417 (1978).
[42] T. H. J. de Reus, J. Reinhardt, B. Müller, W. Greiner, G. Soff, and U. Müller, J. Phys. B **17**, 615 (1984).
[43] E. Ackad and M. Horbatsch, Phys. Rev. A **78**, 062711 (2008).
[44] Th. Stöhlker *et al.*, Phys. Lett. A **238**, 43 (1998).
[45] Th. Stöhlker *et al.*, Phys. Rev. A **57**, 845 (1998).
[46] D. C. Ionescu and Th. Stöhlker, Phys. Rev. **67**, 022705 (2003).
[47] M. Rotenberg, Adv. At. Mol. Phys. **6**, 233 (1970).
[48] P. F. Gruzdev, G. S. Soloveva, and A. I. Sherstyuk, Opt. Spectrosc. **63**, 1394 (1987).
[49] N. L. Manakov, L. P. Rapoport, and S. A. Zapryagaev, Phys. Lett. A **43**, 139 (1973).

[50] G. W. F. Drake and S. P. Goldman, Adv. At. Mol. Phys. **25**, 393 (1988).
[51] J. Avery and F. Antonsen, J. Math. Chem. **24**, 175 (1998).
[52] I. P. Grant and H. M. Quiney, Phys. Rev. A **62**, 022508 (2000).
[53] I. I. Tupitsyn, V. M. Shabaev, J. R. Crespo López-Urrutia, I. Draganic, R. S. Orts, and J. Ulrich, Phys. Rev. A **68**, 022511 (2003).
[54] I. I. Tupitsyn, A. V. Volotka, D. A. Glazov, V. M. Shabaev, G. Plunien, J. R. Crespo López-Urrutia, A. Lapierre, and J. Ullrich, Phys. Rev. A **72**, 062503 (2005).
[55] P. O. Löwdin, Adv. Phys. **5**, 1 (1956).
[56] S. Kotochigova and I. Tupitsyn, Int. J. Quantum Chem. **56**, 307 (1995).
[57] I. I. Tupitsyn, D. A. Savin, and V. G. Kuznetsov, Opt. Spectrosc. **84**, 344 (1998).
[58] L. Yang, D. Heinemann, and D. Kolb, Chem. Phys. Lett. **178**, 213 (1991).
[59] O. Kullie and D. Kolb, Eur. Phys. J. D **17**, 167 (2001).
[60] V. I. Lisin, M. S. Marinov, and V. S. Popov, Phys. Lett. B **69**, 141 (1977).
[61] V. I. Matveev, D. U. Matrasulov, and H. Yu. Rakhimov, Phys. At. Nucl. **63**, 318 (2000).
[62] B. Müller and W. Greiner, Z. Naturforsch. **31a**, 1 (1976).
[63] V. I. Lisin, M. S. Marinov, and V. S. Popov, Phys. Lett. B **91**, 20 (1980).
[64] V. S. Popov, Phys. At. Nucl. **64**, 367 (2001).
[65] J. Crank and P. Nicholson, Proc. Cambridge Philos. Soc. **43**, 50 (1947).
[66] M. D. Feit, J. A. Fleck, Jr., and A. Steiger, J. Comput. Phys. **47**, 412 (1982).
[67] J. Wilkinson and C. Reinsch, *Handbook for Automatic Computation* (Springer-Verlag, Berlin, 1971).
[68] I. P. Grant and B. L. Gyorffy, in *The Effects of Relativity in Atoms, Molecules, and the Solid State*, edited by S. Wilson (Plenum, New York, 1991).
[69] R. Szmytkowski, J. Phys. B **30**, 825 (1997).
[70] I. P. Grant, Adv. Phys. **19**, 747 (1970).
[71] V. F. Bratsev, G. B. Deyneka, and I. I. Tupitsyn, Bull. Acad. Sci. USSR, Phys. Ser. **41**, 173 (1977).
[72] R. R. Sharma, Phys. Rev. A **13**, 517 (1977).
[73] M. E. Rose, *Relativistic Electron Theory* (Wiley, New York/London, 1961).
[74] D. A. Varshalovich, A. N. Moskalev, and V. K. Khersonskii, *Quantum Theory of Angular Momentum* (World Scientific, Singapore, 1988).
[75] J. E. Marsden and A. J. Tromba, *Vector Calculus*, 5th ed. (W. H. Freeman, New York, 2003).
[76] E. U. Condon and G. H. Shortley, *Theory of Atomic Spectra* (Cambridge University Press, London, 1935).
[77] D. R. Bates and R. McCarroll, Proc. R. Soc. London A **245** 175 (1958).
[78] P. O. Löwdin, J. Chem. Phys. **18**, 365 (1950).
[79] G. W. Pratt Jr. and S. F. Neustadter, Phys. Rev. **101**, 1248 (1956).
[80] V. M. Shabaev, I. I. Tupitsyn, V. A. Yerokhin, G. Plunien, and G. Soff, Phys. Rev. Lett. **93**, 130405 (2004).
[81] I. I. Tupitsyn and V. M. Shabaev, Opt. Spectrosc. **105**, 183 (2004).
[82] F. A. Parpia and A. K. Mohanty, Chem. Phys. Lett. **238**, 209 (1995).
[83] L. LaJohn and J. D. Talman, Theor. Chim. Acta. **99**, 351 (1998).
[84] A. Rutkowski, Chem. Phys. Lett. **307**, 259 (1999).
[85] B. Müller, J. Rafelski, and W. Greiner, Z. Phys. **257**, 183 (1972).
[86] M. S. Marinov, V. S. Popov, and V. L. Stolin, J. Comput. Phys. **19**, 241 (1975).
[87] K.-H. Wietschorke, B. Müller, W. Greiner, and G. Soff, J. Phys. B **12**, L31 (1979).
[88] F. A. Parpia and A. K. Mohanty, Phys. Rev. A **46**, 3735 (1992).
[89] I. Angeli, At. Data Nucl. Data Tables **87**, 185 (2004).
[90] Y. S. Kozhedub and V. M. Shabaev (unpublished).
[91] Y. S. Kozhedub, O. V. Andreev, V. M. Shabaev, I. I. Tupitsyn, C. Brandau, C. Kozhuharov, G. Plunien, and T. Stöhlker, Phys. Rev. A **77**, 032501 (2008).
[92] W. R. Johnson and G. Soff, At. Data Nucl. Data Tables **33**, 405 (1985).
[93] W. Fritsch and C. D. Lin, Phys. Rev. A **26**, 762 (1982).
[94] H. J. Lüdde and R. M. Dreizler, J. Phys. B **14**, 2191 (1981).
[95] H. J. Lüdde and R. M. Dreizler, J. Phys. B **15**, 2703 (1982).
[96] R. Shakeshaft, Phys. Rev. A **18**, 1930 (1978).
[97] R. K. Janev and J. J. Smith, At. Plasma Mater. Interact. Data Fusion, Nucl. Fusion Suppl. Special Issue **4** (1993).
[98] M. B. Shah, J. Phys. B **20**, 2481 (1987).
[99] M. B. Shah, J. Phys. B **31**, L757 (1998).
[100] V. P. Shevelko, (private communication).
[101] V. P. Shevelko, I. Yu. Tolstikhina, and Th. Stöhlker, Nucl. Instrum. Methods B **184**, 295 (2001).
[102] R. Schuch, H. Ingwersen, E. Justiniano, H. Schmidt-Böcking, M. Schulz, and F. Ziegler, J. Phys. B **17**, 2319 (1984).
[103] R. Schuch, M. Meron, B. M. Johnson, K. W. Jones, R. Hoffmann, H. Schmidt-Böcking, and I. Tserruya, Phys. Rev. A **37**, 3313 (1988).
[104] S. Hagmann, C. L. Cocke, J. R. Macdonald, P. Richard, H. Schmidt-Böcking, and R. Schuch, Phys. Rev. A **25**, 1918 (1982).
[105] S. Hagmann *et al.*, Phys. Rev. A **36**, 2603 (1987).